THE INFLUENCE OF CLIMATE AND TECTONICS ON TOPOGRAPHY IN THE HAYES RANGE AND ITS FOOTHILLS

By

Gabrielle T. Vance

RECOMMENDED:

Dr. Elisabeth Nadin

Dr. James Beget

Dr. Wesley Wallace
Advisory Committee Chair

Dr. Paul McCarthy
Chair, Department of Geology and Geophysics

APPROVED:

Dr. Paul Layer
Dean, College of Natural Science and Mathematics

Dr. John Eichelberger
Dean of the Graduate School

11/25/13
Date

THE INFLUENCE OF CLIMATE AND TECTONICS ON TOPOGRAPHY IN THE HAYES RANGE AND ITS FOOTHILLS

A

THESIS

Presented to the Faculty

of the University of Alaska Fairbanks

in Partial Fulfillment of the Requirements

for the Degree of

MASTER OF SCIENCE

By

Gabrielle T. Vance, B.A.

Fairbanks, Alaska

December 2013

Abstract

Complex feedback exists among climate, tectonics, and glacial erosion in the creation of topography: climate influences glaciation; tectonics and glacial erosion modify topography; topography influences climate. The objectives of this study are to determine elevation distribution in the Hayes Range area of the central Alaska Range and to identify evidence for structural or erosional controls. I have used geospatial information systems (GIS) software to map mean elevation, calculate geomorphic indices from a digital elevation model (DEM), and characterize climatic, tectonic, and topographic patterns. Deformation, elevation, and erosion all increase southward within the range. In the northern part of the range, Quaternary doubly plunging anticlines and thrust faults uplift and deform a relict landscape. Despite the dominance of fluvial erosion, these elliptical topographic highs are tectonically controlled. Similar larger elliptical topographic highs are present farther into the range to the south, but Quaternary structures are more difficult to identify because of greater glaciation and erosion. The study area is one of high mean elevation, summits, slope, and relief. Topography in the Hayes Range exceeds what would be expected if glacial erosion kept pace with rock uplift. A young antiform in the Hayes Range can account for the rapid rock uplift needed.

Table of Contents

Page

List of Figures

Page

List of Tables

Page

Acknowledgments

The Alaska Geological Society, Sigma Xi, NASA's Eyes on the Arctic, and the National Science Foundation Changing Alaska Science Education (CASE) GK-12 Fellowship provided financial support for this project. Many thanks to Casey Denny for the 10 m DEM, Christian Kienholz for scripting, and Jill Carlile for field assistance. While I did the majority of the research and writing for this paper, I would especially like to thank my advisor and co-author Wes Wallace for all his help.

Introduction[1]

Climate influences glaciation, glaciation and tectonics modify topography, and topography influences climate (e.g., Molnar and England, 1990; Koons, 1994; Anders et al., 2010). Tectonically active, glaciated mountain ranges such as those in south-central Alaska illustrate this complex feedback system particularly well. For example, Meigs and Sauber (2000) have characterized climatic, tectonic, and topographic patterns in southern Alaska, including the Alaska Range. I have applied a similar approach to the east-central Alaska Range between the Wood and Delta Rivers (Fig. 1). This includes an area of >4200 m elevation from Mount Deborah to McGinnis Peak, with its highest point at Mount Hayes. For simplicity I will refer to this region as the Hayes Range.

The relationship between tectonics and erosion in creating topography is a complex one. Molnar and England (1990) characterized mountain building and climate change (and associated erosion) as a "chicken or egg?" problem: does the formation of topography result in climate change, or vice versa? It turns out that for the Hayes Range, it is not possible to answer this question directly. Instead, I assess the relative roles of climate and tectonics in the creation of topography.

Koons (1994) argued that erosion and tectonic processes drive the evolution of mountainous topography, with structural control of erosional regime and thus of valley and ridge formation. Other authors link erosional patterns, deformation, and

---

[1] Vance, G., and W. Wallace, 2013. The influence of climate and tectonics on topography in the Hayes Range and its foothills. Prepared for submission to Journal of Quaternary Research.

topographic form in active orogens (e.g., Meigs and Sauber, 2000). Citing thermochronometric data, Meigs and Sauber (2000) posited that structure controls topographic texture, e.g., the distribution of high peaks. They also argue that deformational patterns control topographic change at multiple scales, from individual structures to the entire orogen (Meigs and Sauber, 2000).

The interactions of climate, tectonics, and erosion in the creation of topography are complex and interdependent. The Dictionary of Geological Terms defines topography as "the general configuration of a land surface, including its *relief* and the position of its natural and man-made features" (Bates and Jackson, 1984). Relief refers to "the elevations or differences in elevation, considered collectively, of a surface," and elevation to "the vertical distance from mean sea level to a point or object on the Earth's surface; height above sea level" (Bates and Jackson, 1984). The ESRI GIS Dictionary defines slope as "the incline, or steepness, of a surface," in this case, the ground, "measured in degrees from horizontal (0–90)."

For the purposes of this study, "topography" refers to both elevation (which controls whether glaciers are present) and relief (which is important in understanding evolution and process). The interplay between rock uplift and exhumation creates topography: surface uplift = rock uplift – exhumation (Molnar and England, 1990). Both rock uplift and exhumation influence elevation change (surface uplift); the creation of relief (differential exhumation) can also produce local surface uplift through isostatic adjustment.

Climate plays a complex role in the formation of topography**.** In the Hayes Range, erosion is the main cause of exhumation. Erosion is controlled by climate (precipitation, temperature), rock type (erodibility), and rock uplift. Active deformation may cause thickness and/or density changes that result in increased elevation and consequent increased erosion.

Erosional exhumation may persist as a result of isostatic rock uplift where previous tectonic activity has changed thickness and/or density with respect to background levels.

In areas of active deformation, tectonism and erosion produce dramatic relief. The northwestern Himalaya is a prime example of such interactions. There, Brozovic et al. (1997) found that glaciers limit the development of topography regardless of tectonic activity. Mitchell and Montgomery (2006) referred to this important concept as the "glacial buzzsaw." Anders et al. (2010) found that in the Swiss Alps, climate limits topography to altitudes near the equilibrium line altitude (ELA). The glacial buzzsaw hypothesis remains controversial, although it is supported by studies in the Basin and Range, Cascade Range, Chugach Range, Himalaya, and Kyrgyz Range (Anders et al., 2010). These studies correlate peak elevations with snowlines, exhumation rates with glacial extent, and landscape evolution with glacial erosion. In contrast to the glacial buzzsaw, the "Teflon peaks" hypothesis states that steep peaks shed snow or ice, protecting them from glacial erosion and promoting the growth of local relief (Ward et al., 2012).

A glacier's equilibrium line altitude (ELA) marks where accumulation and ablation of glacier ice are in equilibrium (Péwé, 1975). ELAs of modern glaciers can be measured and contoured with some accuracy, but reconstructed ELAs of past glaciers are more approximate indices that can be derived from studies of previous glacial extent. Regional snowlines serve as a proxy for regional ELAs, since ELAs are sensitive to minor topographic and climatic changes and vary considerably even when calculated for a single glacier (Brozovic et al., 1997; Péwé, 1975). In the northwest Himalaya, Meigs and Sauber (2000) suggested that the mean position of the ELA, where glacial erosion is especially effective, controls topography.

Fluvial erosion tends to produce landscapes with predictably smooth, concave power-law longitudinal profiles (Brocklehurst and Whipple, 2006) and V-shaped valley cross sections (Brook et al., 2006). Glacial erosion widens and incises fluvial valleys, flattening long profiles (MacGregor et al., 2000) and creating U-shaped cross sections (Brocklehurst and Whipple, 2006). This characteristic U-shape results from the locus of basal sliding and glacial erosion moving away from the center of a previously V-shaped valley (Harbor, 1992). Numerical models like that of MacGregor et al. (2000) and comparative field studies show that glacial erosion removes larger volumes of rock than fluvial erosion, while studies in New Zealand's Southern Alps (e.g., Brook et al., 2006) suggest that glacial erosion is faster than fluvial erosion in rapidly uplifting ranges. Comparison of Himalayan fluvial and glacial basins under similar climatic and tectonic conditions highlights the ability of glacial erosion to keep pace with rapid uplift, unlike fluvial erosion (Brocklehurst

and Whipple, 2006). In the Nanga Parbat region of the Himalaya in Pakistan, Brozovic et al. (1997) determined that glaciated landscapes had similar snowlines regardless of their varying exhumation rates, a result of glacial erosion keeping pace with rapid uplift. Montgomery et al. (2001) concluded that the high Andes, too, are subject to a glacial buzzsaw, where effective glacial erosion limits the development of relief.

Drainage patterns are particularly responsive to active tectonics (Schumm, 1986). In the Siwalik foothills of northwest India, Delcaillau et al. (2006) analyzed landform topography and river incision to identify actively growing anticlines and faults. Their approach included spatial mapping of drainage patterns, scarps, uplifted alluvial fans, and along-strike changes in ridge morphology, as well as calculating geomorphic parameters (Delcaillau et al., 2006). Similarly, Ramsey et al. (2008) used topographic contours, relict drainage patterns, and ridge crest profiles to describe actively growing folds in the Zagros of Iran.

The expression of active structures in glaciated regions is difficult to assess, since glaciers obscure much of the evidence. Recent work in the St. Elias Range (e.g, Berger et al., 2008; Spotila and Berger, 2010) and New Zealand's Southern Alps (e.g., Whipple, 2009; Tomkin and Roe, 2007) addresses the tectonically active, glaciated orogens at a regional scale rather than the scale of individual structures. The question remains, can uplift by an active tectonic structure outpace glacial erosion?

In their 2000 study, Meigs and Sauber posed two central questions: "What is the topographic form of an active orogenic belt whose erosion has been dominated

by glaciers? How do topographic characteristics relate to tectonic and climatic patterns?" I apply a similar question to the tectonically active Hayes Range: what are the relative contributions of active tectonics and erosion to the creation of elevation and relief in the Hayes Range study area? This area of high topography has been studied (e.g., Benowitz et al., 2011 and 2013), but less than the high topography of the Denali massif in the western Alaska Range (e.g., Fitzgerald et al., 1995; Haeussler, 2008; Ward et al., 2012).The main objective of my study is to quantitatively assess topography by determining mean elevation distribution in the Hayes Range, and to identify evidence for climatic and/or tectonic controls on topography, particularly the role of glaciation in shaping topography. I have used regional-scale digital elevation models and remote sensing to define broad topographic trends, and on-the-ground fieldwork in the Anderson Mountain area of the Wood River valley to provide additional elevation data from a representative topographic high and accompanying diverted drainage.

Regional setting

Southern Alaska is a large region of active orogenesis that lies within the diffuse, convergent Pacific–North American plate boundary (Plafker et al., 1994; Trop and Ridgway, 2007; Haeussler, 2008; Spotila and Berger, 2010). The Alaska Range curves over ~1000 km from the Alaska Peninsula to the Canadian border (Fig. 1). Highs in the Denali massif and the east-central Alaska Range are separated by relatively low topography in the center bounded by an arcuate belt of foothills to the north (Bemis and Wallace, 2007; Bemis et al., 2012). This Northern Foothills

fold-and-thrust belt is a wide zone of multiple thrusts and folds, probably formed above a common regional detachment (Bemis and Wallace, 2007; Bemis et al., 2012).

This study focuses on an area between the Wood and Delta Rivers (Fig. 1). Published 1:250,000 scale geologic maps of this area (Csejtey et al., 1992; Nokleberg et al., 1992) provide little information about recently recognized Quaternary deformation. Bemis et al. (2012) identified a continuous system, ~500 km long, of faults and folds active during the Quaternary on the northern flank of the Alaska Range. In the northern part of the range, Quaternary deformation is clearly defined by the upper surface of the Tertiary Nenana Gravel, which consists of coarse alluvial fan and braidplain deposits, that is uplifted and deformed by doubly plunging anticlines and thrust faults (Bemis and Wallace, 2007; Lesh and Ridgway, 2007; Bemis et al., 2012). A similar distribution of elliptical topographic highs is present farther south, but Quaternary structures are more difficult to identify here because of increased glaciation and erosion (Fig. 2).

Methods

In this study, I combine regional landscape analysis with targeted fieldwork to describe distribution of elevation in the Hayes Range. I use satellite imagery, digital elevation models (DEMs), and geographic information systems (GIS) software to determine mean elevation, extract topographic profiles, and calculate geomorphic indices such as stream length-gradient indices and valley width/height ratios.

Average elevation and relief

My approach for analyzing mean elevation in the Hayes Range is similar to that applied by Meigs and Sauber (2000) to the Chugach/St. Elias range. I used the statistics capabilities of ArcGIS to calculate mean elevation from a 10 m resolution radar-based DEM (courtesy of Casey Denny, Geographic Information Network of Alaska; Fig. 3). Meigs and Sauber's (2000) technique employs a square window (30 x 30 data points) that scrolls, pixel by pixel, over the entire elevation data set. Mean elevation is the sum of the window's elevations divided by the number of data points it contains (Meigs and Sauber, 2000). I started by resampling the 10m DEM at 100-m intervals, in order to reduce noise. I then used a circular window with a radius of 200 data points (radius ~2 km, covering a ground area of ~12 km^2) to calculate mean elevation**.** I used this size window because it provided the optimum balance among filtering, level of detail, and processing intensity. Figure 4 shows the resulting mean elevation map, while Figure 5 includes contours of mean elevation.

I used "interpolate line" in ArcGIS to extract seven south–north topographic profiles, spaced by ~20 km, from the DEM and map of mean elevation. I exported the distance and elevation data to Excel, which I used to create profile graphs (Figs. 6, 7).

I used ArcGIS statistics and Excel to plot a hypsometric curve, which shows regional elevation distribution (Fig. 8). I found the average elevation along each S-N topographic profile, and plotted these values longitudinally using Excel (Fig. 9a). I also plotted the maximum relief (difference between highest and lowest elevation)

of each S-N profile (Fig. 9b). I used the "ruler" tool in ArcGIS to measure the width of topographic highs, then plotted the average width for each S-N profile (Figure 9c).

I used "interpolate line" in ArcGIS to measure mean elevation along W–E profiles, segments chosen to correspond to areas dominated by fluvial erosion and by glacial erosion, and an area transitional between these two modes (Fig. 10). I also used ArcGIS to create a regional slope map (Fig. 11) and plot slope/altitude distribution (Fig.12).

Active tectonics

I used satellite imagery to identify active antiforms, outlining areas of high topography and accompanying diverted drainages (Fig. 2). I compiled the structures identified by Bemis et al. (2012) and the newly identified antiforms on my structural reference map (Fig. 3).

Erosion

ELAs

The ideal way to determine a glacier's ELA is direct mass balance measurement over several years, but this approach requires extensive fieldwork (Péwé, 1975). A technique more feasible for my study area was the accumulation area ratio (AAR), which assumes that the accumulation area of a glacier accounts for a certain percent of its total area, for example, 60% or more in healthy glaciers (Péwé, 1975). I used an accumulation area ratio of 67% of total glacier area, and used a Python script to determine the elevations above which 67% of each glacier's surface area exists above that elevation (Kienholz, personal comm., 2013). I

obtained the extent and area of modern glaciers from the Randolph Glacier Inventory (RGI), a dataset of global glacier outlines (Arendt et al., 2013). I determined AAR ELA values and used ArcGIS to interpolate and contour an ELA surface (Fig. 13).

I also used the toe-summit altitude method (TSAM) to calculate modern and Last Glacial Maximum (LGM) ELAs. I identified terminal moraine complexes that are clearly visible in satellite imagery. The TSAM places the ELA halfway between a glacier's toe elevation and that of the highest peak in its catchment area, so I averaged the two elevations to find the value of the ELA. Again, I used ArcGIS to interpolate and contour modern and LGM TSAM ELA surfaces (Figs. 14, 15). I compared my calculated ELAs to those determined by Péwé (1975) (Fig. 16). My analysis of glacial erosion is based on that of Anders et al. (2010) in the Swiss Alps: contouring the modern ELA and comparing it to means of elevation, annual precipitation, and annual temperature.

Climatic trends

I used the PRISM climate model to assess modern temperature and precipitation trends (Daly et al., 1994). PRISM interpolates weather station data to produce a map of monthly average precipitation and temperature data across Alaska. I imported this map into ArcGIS, sampled precipitation and temperature data on profiles across the Hayes Range from south to north and along it from west to east using profile line and interpolate graph functions, and exported the profile data to create graphs in Excel (Figs. 17, 18).

Extent of fluvial and glacial erosion

To map the extent of modern fluvial and glacial erosion, I imported the Alaska state hydrology layer, which shows digitized streams and rivers (courtesy of the Geographic Information Network of Alaska, GINA), and the Alaska Paleoglacier Atlas, which shows modern, Late Wisconsin, and maximum glacial extents (Manley and Kaufman, 2002), into ArcGIS (Figs. 19, 20). I compared fluvial and glacial extents to mean elevation (Fig. 21).

Geomorphology

The Hayes Range includes a fluvial-dominated landscape in the Tanana flats north of the Alaska Range, a fluvial-glacial landscape in the northern foothills, and a glacial landscape in the high peaks, so it was necessary to apply geomorphic indices to examine the different, and combined, effects of fluvial and glacial processes on topography. I identified valley types (fluvial, glacial, or mixed) and summarized and compared geomorphic characteristics of major drainages in the Hayes Range. From west to east these are the Wood River, West Fork Little Delta River, East Fork Little Delta River, Delta Creek, and Delta River (Fig. 2).

I used a handheld GPS unit to measure a cross-valley profile and a portion of the longitudinal profile of the Wood River in the field, and extracted the same profiles from the DEM in ArcGIS (Figs. 22, 23). I extracted the rest of the cross-valley and longitudinal profiles from the DEM in ArcGIS using the “interpolate line”

feature, then exported the elevation data to create profile graphs in Excel (Figs. 24-29).

I calculated a series of V ratios to describe valley shapes: the valley floor width-to-height ratio (V_f), ratio of valley width-to-height (V), and valley shape/circularity (V_c) (Fig. 30). To calculate these ratios, I used valley profile graphs extracted from the 10 m DEM using the ArcGis "interpolate line" and "profile graph" features. The valley floor width-to-height ratio (V_f) is:

$$V_f = 2V_{fw}/[(A_{rd}-A_{sc})+(A_{ld}-A_{sc})] \quad (1)$$

where V_{fw} is the valley floor width, A_{sc} is the altitude of the stream channel, and A_{rd} and A_{ld} are the altitudes of the and left drainage divides, all in meters, from the 10m DEM (Burbank and Anderson, 2011). $V_f > 1$ signifies a U-shaped valley and $V_f < 1$ indicates a V-shaped valley (Burbank and Anderson, 2011). I extracted valley profile graphs from the 10 m DEM using the ArcGis "interpolate line" and "profile graph" features. I calculated the ratio of valley width-to-height (V):

$$V = 2V_w/[(A_{rd}-A_{sc})+(A_{ld}-A_{sc})] \quad (2)$$

where V_w is the width of the entire valley, from drainage divide to drainage divide, A_{sc} is the altitude of the stream channel, and A_{rd} and A_{ld} are the altitudes of the right and left drainage divides (viewed downstream), all in meters (Burbank and Anderson, 2011). I also measured valley shape/circularity (V_c):

$$V_c = A_v/A_c \quad (3)$$

where A_v is a cross-sectional area of the valley and A_c is a semicircular area with radius equal to valley height (both in m^2) (Burbank and Anderson, 2011).

Changes in stream gradient along a longitudinal profile reflect changes both in stream power and channel slope (Chen et al., 2003). Longitudinal stream profiles plot height vs. distance from the river head, as shown in Figures 27-29. Logarithmic patterns indicate passive, tectonically undisturbed streams and convex-upward longitudinal profiles generally reflect high uplift rates (Chen et al., 2003). I measured longitudinal profiles of the main drainages of the Hayes Range using "interpolate line" from the 10 m DEM and hydrology layer in ArcGIS. From the longitudinal profiles of the major drainages, I derived semilogarithmic plots or Hack profiles (Chen et al., 2003). The absolute value of the slope of the Hack profile is the stream gradient index, k, which I measured directly from my Excel graphs.

Lesh and Ridgway (2007) also show longitudinal profiles for the major drainages in the Hayes Range study area: Wood River, Little Delta River, and Delta River. Others have done similar work nearby, including Denny (2013) and Bemis and Wallace (2007), who show longitudinal profiles of north-flowing streams from the Nenana River to Tatlanika Creek, an area west of the Hayes Range study area.

Rock type

I used the Geologic Map of Central (Interior) Alaska (Wilson et al., 1998) for information about rock types present in the Hayes Range study area (Fig. 31).

Drainage divides and peaks

I identified drainage divides within the Hayes Range using the Alaska state hydrology layer (courtesy of GINA), which I imported into ArcGIS. Inspired by Spotila (2012), I inspected peaks using 3-D visualization of digital topography, in my

case, a hillshade derived from the 10 m DEM, to determine their distribution with respect to local drainage divides. I combined the hydrology layer and hillshade to produce a drainage divide map (Fig. 32).

Ridge profile

I used "interpolate line" in ArcGIS to measure a topographic profile along a continuous ridgeline across the inferred fold trend. I chose the western ridgeline through mounts Balchen, Geist, and Giddings because it appeared to be one of the most continuous and least dissected (Fig. 32). I exported the elevation data into Excel to create the ridge profile graph (Fig. 33).

Results

Average elevation and relief

The Hayes Range hypsometric curve describes regional elevation distribution and was determined using ArcGIS' statistics capabilities (Fig. 8). Mean elevation is 2235 m, above the altitudinal range of the modern ELA (1320–1710 m, as determined using the AAR). Peak elevations exceed 4000 m. As expected for glacial and fluvial landscapes, high peaks occupy only a small percentage of the total area (Meigs and Sauber, 2000).

Comparing the topographic and mean elevation profiles shows several general trends in landscape form. Mean range height for each of the S-N profiles shows little variation in mean elevation along strike, averaged across the entire foothills belt (Fig. 9a, Table 1). The Delta River's transverse drainage corresponds to the easternmost topographic low (Fig. 9a).

Width of topographic highs determined from S-N profiles is greatest (~20 km) in the center of the study area, decreasing toward the east and west ends (Fig. 9b, Table 1). In contrast, relief is greatest (~1500 m) near the eastern end of the area studied, in the cluster of summits east of Mount Hayes and west of McGinnis Peak, between the Denali and Trident Glacier faults (Fig. 9c, Table 1).

Figure 10 shows that the maximum elevation is in the eastern part of the glaciated segment and that the topographic high shifts westward approaching the range front. Mean elevation is lowest along the fluvial segment, with a slight peak towards the western end of the study area. Mean elevation along the transitional segment is highest in the foothills north of Mount Deborah (Fig. 10), while along the glaciated segment it is highest in the vicinity of Mount Hayes itself.

The regional slope/altitude distribution curve (Fig. 12) shows a central plateau with slope values of ~18–20° (50^{th} percentile) between 1300 and 3200 m elevation, with decreasing slope at higher and lower elevations. The area of the Hayes Range between the Denali fault and the arcuate northern edge of the Hayes Range topographic high has particularly high elevation and slope, in contrast to neighboring broad, low-elevation glacial valleys (Fig. 11).

Active tectonics

Regional topography of the Hayes Range and its foothills between the Wood and Delta Rivers shows a series of elliptical highs trending WNW–ESE, around which glacial and river valleys are diverted (Fig. 2).

Erosion

ELAs

The range of calculated modern AAR ELAs is 1320–1710 m. Contours of the modern AAR ELA (Fig. 13) define a complex southeast-striking, southwest-facing surface that climbs ~5 m/km, from 1400 m at the west end of the study area to 1700 m at the east end over a distance of ~60 km, for a total of 300 m. ELAs climb from west to east, then decrease again east toward the Delta River. Plotting the altitudinal range of the modern ELA on the Hayes Range hypsometric curve shows that slightly less than 40% of the modern landscape lies at or above the 1320 m ELA (Fig. 8). Summit elevations are ~2000 m higher than the ELA. Calculated ELAs are summarized in Tables 2, 3, and 4.

Climatic trends

As expected for a coastal–continental transitional range, mean annual precipitation is higher on the southern, windward side of the Hayes Range (800–1300 mm/year), reaches a maximum (1495 mm/year) at the range crest, and drops precipitously on the northern, leeward side (<400 mm/year) (Fig. 17) (Daly et al., 1994). This orographic rain- or snow-shadow effect is typical of high ranges proximal to coasts (Meigs and Sauber, 2000). Also as expected, mean annual temperature reaches a local minimum (~-16° C) at the highest elevations of the central Hayes Range, is -4 to -8 ° C in the maritime climate south of the range, and is slightly warmer (-2 to -6 ° C) on the drier leeward side (Fig. 17) (Daly et al., 1994).

Along a west–east transect, regional temperature and precipitation patterns are more complex. The highest precipitation (~1400–1600 mm/year) and lowest mean annual temperature (~-16 ° C) correspond to the high summits from Mount Hayes to Mount Moffit (Fig. 18), between about 50 to 90 km east of Wood River (Daly et al., 1994).

Extent of fluvial and glacial erosion

The Hayes Range is along part of the larger Alaska Range drainage divide between the Yukon system on the north side and the Gulf of Alaska on the south side (Fig. 1). The Wood and Delta Rivers (and major drainages in between) flow northward to join the Tanana River and from there flow into the Yukon River (Figs. 1, 2). At the west end of the Hayes Range study area, the roughly range-parallel Yanert and Nenana Glaciers drain into the Nenana River, which is also a tributary of the Tanana (Figs. 1, 13). The glaciers in the central part of the southern side of the Hayes range—West Fork, Susitna, and Maclaren—drain into tributaries of the Susitna River, which flows south to Cook Inlet, the Gulf of Alaska, and the Pacific Ocean (Figs. 1, 13). The Eureka and other easternmost glaciers on the southern side of the Hayes Range drain into the Delta River, which flows north to the Tanana. The Black Rapids Glacier, which is parallel to the range, also drains into the Delta River (Figs. 1, 13). Most notably, the drainage patterns of both fluvial and glacial valleys outline a series of elliptical topographic highs, exemplified by the Wood River's diversion around Anderson Mountain on the west side (Fig. 2).

The modern Hayes Range has sizable valley glaciers—more extensive on the south side, consistent with precipitation patterns—as well as numerous smaller alpine glaciers (Fig. 19). At their maximum extent, the glaciers on the northern side of the Hayes Range covered a considerable portion of the southern Yukon-Tanana basin; the individual modern glaciers are remnants of several main complexes: Wood River, Gillam, and a Trident-Black Rapids-Delta River piedmont glacier (Manley and Kaufman, 2002; Fig. 20).

Geomorphology

GPS-based and DEM-derived cross-valley profiles of the Wood River and other major drainages of the Hayes Range demonstrate a strong glacial signature to the topography: despite more recent fluvial erosion, valleys are distinctly U-shaped (Figs. 24-26), with the exception of the markedly V-shaped West Fork Little Delta River valley.

Calculations of V_f confirm this qualitative assessment of topography. As expected, the more U-shaped Wood River, East Fork Little Delta River, Delta Creek, and Delta River valleys have higher V_f values, while the V-shaped West Fork Little Delta River valley has a lower V_f (Table 5), suggesting that stream incision is the main factor controlling its shape. The same pattern holds for other calculated geomorphic indices, which all group together with high values of valley width-to-height ratios and valley semicircularity except for the West Fork Little Delta River (Tables 6, 7).

Measured longitudinal profiles show neither logarithmic patterns nor convex-upward profiles. Instead, they are relatively straight (Figs. 27-29). The longitudinal profiles I graphed also show numerous anomalies (Figs. 27-29). The anomalies, upward jumps that gradually decay downward to the actual profile, do not appear to contain any useful information. Their chaotic nature and small size (m scale) suggest they are simply DEM artifacts of some kind. I use dashed lines to show the inferred profiles across the anomalies, continuing a smooth, normal gradient. This approach, though useful, is arbitrary and unconstrained: I estimated what the appropriate gradient should be and assumed that it is not modified by tectonics.

Stream gradient indices, i.e., k values, decrease from west to east (Table 8).

Rock type

High topography is not preferentially located over resistant rock types that lack a significant structural overprint (i.e., undeformed plutons). It is equally well developed in erodible sedimentary and metasedimentary rocks (Fig. 31).

Drainage divides and peaks

The distribution of drainage divides (e.g., Oskin and Burbank, 2005) and peaks (e.g., Spotila, 2012) helps identify relict landscapes and how drainages relate to them. Drainage divides within the Hayes Range separate the area into a narrow, steep area just north of the Denali fault and a wide, incised area farther north. The local direction of drainage does not necessarily reflect where the drainages end up: drainages to the south end up in the Nenana, Susitna, and Delta Rivers, and to the

west end up in the Nenana and Wood Rivers (Fig. 32). All of the named peaks in excess of 3000 m are at or north of the divide.

Ridge profile

North-trending ridges show remnants of the original erosion surface, especially at or near peaks along the ridgeline. The measured ridge profile shows an upward convex curvature (Fig. 33).

Discussion

Average elevation and relief

The dramatic relief between the high summits and major glacial valleys may reflect high uplift rates due to north–south contraction between the Denali and Hines Creek faults (Hickman et al., 1990; Csejtey et al., 1992; Nokleberg et al., 1992; Ridgway et al., 2002). The area of the Hayes Range between the Denali fault and the arcuate northern edge of the Hayes Range topographic high has particularly high elevation and slope, in contrast to neighboring broad, low-elevation glacial valleys. This suggests a growing structure around which major drainages, both fluvial and glacial, were diverted. Variation in width of topographic highs, particularly the increase in width moving southward into the glaciated Hayes Range, reflects the dominant influence of this elliptical Hayes Range antiform, which may be bounded to the north by an arcuate thrust fault (Fig. 2).

Elevation distribution varies considerably along strike with distance from the range front (Fig. 10), but is relatively constant along strike, except in the Delta River Valley, averaged across the foothills (Fig. 9a). If elevation is linked to

structure, the differing spatial patterns of elevation shown by Figure 9a and Figure 10 imply that shortening is distributed differently along different lines across the Northern Foothills fold and thrust belt.

Active tectonics

I interpret the elliptical highs trending WNW–ESE, around which glacial and river valleys are diverted (Fig. 2), to represent doubly plunging anticlines, for the following reasons. Regional drainage patterns show clear deflections around the elliptical highs, as expected for streams flowing around actively growing structures (e.g., Ramsey et al., 2008). The distribution of these topographic highs does not correlate directly with that of more resistant rock types (Fig. 31). Elliptical topographic highs correspond with young anticlines identified by Bemis et al. (2012) at the range front, where the upper surface of the Nenana Gravel is uplifted and folded (Japan Hills, range-front monocline, Rex anticline, as shown in Fig. 2).

The Glacier Creek antiform (Fig. 2) stands out as an example of a well-defined elliptical topographic high that is a young anticline based on the mapped geology and the fluvial drainage patterns (e.g., Delcaillau et. al, 2006; Ramsey et al., 2008). Young clastic deposits wrap around a higher-elevation schist core on its north side and east and west ends (Fig. 31), and it is bounded to the north by a fault (Fig. 3). Drainages wrap around its east and west ends, and its west end displays an apparent water gap (Fig. 3). The Anderson Mountain antiform displays similar features, especially the sharp bend of the Wood River around its west end (Fig. 3). The Hayes Range itself is potentially a larger, structurally controlled elliptical high.

The topography and mapped geology suggest a thrust-bounded doubly plunging antiform (Figs. 2, 31). In addition to its obvious topographic expression, the antiform is supported by the distribution of rock units, for example, the uplift of the medium-resistance Yanert Fork sequence (Dy) (Fig. 31), and the inferred northern bounding fault corresponds with faults shown on the maps by Csejtey et al. (1992), Nokleberg et al. (1992), and Wilson et al. (1998).

Erosion

ELAs

The ELAs calculated here are for a very small area, and benefit from consideration in a regional context. Péwé (1975) interpreted previous snowline positions, a proxy for ELA, from cirque floor altitudes throughout Alaska. The modern and LGM ELAs I calculated show similar spatial patterns to those calculated by Péwé (1975) (Fig. 16), who found that the LGM snowline parallels the modern snowline at a lower elevation throughout Alaska. Both regionally and locally, the increase in modern and LGM ELAs from the west and south to the east and northeast shows the influence of precipitation on snowline (Péwé, 1975). Along the west-east climate transect, precipitation maxima coincide with the greatest extent of paleoglaciers (Figs. 18, 20).

Geomorphology

The U-shaped cross-valley profiles suggest recent and pervasive glacial influence; even recent uplift and incision have not yet altered them significantly. The West Fork Little Delta River may be incising faster than other drainages due to

increased surface uplift as a result of tectonic activity. All of the other profiles are located across the former paths of major valley glaciers (Fig. 19), but only the West Fork Little Delta River profile is located on an ice gap, across the middle of the proposed Anderson Mountain antiform. The Wood River and East Fork Little Delta River profiles are similarly surrounded by high topography, but they are at the ends of the antiform along its south flank.

The measured longitudinal profiles of the main drainages show neither the logarithmic patterns typical of passive, tectonically undisturbed streams nor the convex-upward profiles associated with high rates of uplift. They are relatively straight (Figs. 27-29), possibly because the profile is controlled by glacial rather than fluvial erosion in these drainages. However, the DEM artifacts present in the profiles are a source of error and limit my interpretation of them. Decreasing values of the stream gradient index, k, suggest that tectonic perturbation of the rivers' longitudinal profiles decreases from west to east, from Wood River to Delta River (Table 8).

Rock type

The "glacial buzzsaw" hypothesis states that glaciers rapidly erode terrain raised above the ELA, causing elevation of tectonically active, glaciated orogens to correlate with ELA. In contrast, the "Teflon peaks" hypothesis states that steep peaks shed snow or ice, protecting them from glacial erosion and promoting the growth of local relief (Ward et al., 2012). Citing greater rock strength and uplift rates of the granitic Denali massif, Ward et al. (2012) identified 'Teflon peaks," e.g.,

Denali, localized where resistance to erosion is highest because of rock type and lack of structural overprints. They further described the rest of the Alaska Range as consisting predominantly of erodible sedimentary and metamorphic rocks with local relief of 1000–1500 m, subject to a glacial buzzsaw (Ward et al., 2012). Mount Hayes stands in prominent exception to this trend: at 4216 m, it is the only Alaska Range peak outside of the Denali massif exceeding 4000 m elevation (Ward et al., 2012).

The "Teflon peaks" model does not apply to the Hayes Range. While contact metamorphic overprint could account for these rocks' local resistance to erosion, as is the case in the north peak of Denali, the plutons are not widely enough distributed for this to account for all of the high topography. There does appear to be some correspondence between plutons and high topography, especially along the Anderson Mountain to Molybdenum Ridge trend (Figs. 4, 5, and 31), but the presence or absence of plutonic rocks does not seem to make much difference on the north and south flanks of the Hayes Range antiform, although perhaps it does along the crest. The elliptical highs from Anderson Mountain to Molybdenum Ridge, identified on Figure 2, trend obliquely with respect to the plutons; more than one elliptical high may be separated by topographic lows within a larger pluton. This, at a more detailed scale, supports the interpretation that the highs are structurally controlled and not simply topographic highs over plutons.

Drainage divides and peaks

The highest peaks are markedly skewed to the north of the north–south drainage divide, suggesting headward erosion toward the south (Fig. 32). A steep, short area north of the Denali fault, but south of the local N-S drainage divide, is the focus of erosion. The south side of the drainage divide is a region of rapid exhumation: the approximately 11 km of exhumation identified by Benowitz et al. (2011) abruptly decreases in amount and rate of exhumation moving northward from the Denali fault. North from the drainage divide, high peaks form a gipfelflur, or remnant erosional surface—although glaciers have dissected it extensively, they have not removed as much material from the ridgelines north of the divide (Fig. 32).

Ridge profile

Peak elevations along ridgelines show a gently convex-upward curvature, as expected if the Hayes massif corresponded with a large antiform (Fig. 33). An envelope over the tops of the ridge defines a smooth curve, supporting the interpretation that the ridgeline reflects a folded paleosurface, similar to what is suggested by Spotila (2012) and by Oskin and Burbank (2005). This may show the interplay between tectonics and glacial erosion: incision and headward erosion in the fault-bounded north limb and crest of the antiform and rapid erosion in the short south limb (Fig. 34).

Concentration of erosion in the south limb may be a result of higher erosion rates due to higher precipitation on the south side combined with structural decoupling and/or southward backthrusting at or near the Denali fault (Fig. 34).

This is consistent with the decrease in cooling ages and increase in exhumation rates southward from the divide toward the Denali fault identified by Benowitz et al. (2011 and 2013). Apatite fission track (AFT) cooling ages decrease from 6.7 to 2.8 Ma from north to south, along a transect across Mount Balchen (Benowitz et al., 2011). K-feldspar minimum cooling ages decrease from 12.8 Ma to 8.5 Ma from north to south approaching the Denali fault (Benowitz et al., 2013). Together, these AFT and K-feldspar minimum cooling ages (Benowitz et al., 2011 and 2013) are older up and to the north away from the Denali fault, indicating a decrease in age of exhumation and an increase in rate approaching the Denali fault. Figure 34 summarizes my interpretation of the regional tectonic setting.

Conclusions

This study identifies and describes the Hayes Range topographic domain between the Wood and Delta Rivers. Mount Hayes (4216 m) is the highest point. Mean elevation is 2235 m, above the altitudinal range of the modern AAR ELA (1320–1710 m). The modern AAR ELA increases ~5 m/km, from west to east, consistent with regional precipitation trends. Slightly less than 40% of the modern landscape lies at or above the ELA. Peak elevations exceed 4000 m, >2000 m higher than the ELA. High peaks occupy only a small percentage of the total area. Slope is greatest, with values of ~18–20° (50th percentile), between 1300 and 3200 m elevation, with decreasing slope at higher and lower elevations.

In the Hayes Range study area, elliptical topographic highs correspond with doubly plunging antiforms and deflect drainages. They are present from the range

front south to the Hayes Range, spanning an area ranging from fluvially to glacially dominated erosion. The area between the Hines Creek and Denali faults is one of high mean elevation, summits, and slope, as well as dramatic relief. The region of high relief and high exhumation north of the Denali fault is likely due to contractional tectonic uplift in the elliptical Hayes Range antiform identified in this study. The glacially dominated Hayes Range antiform has a significantly longer wavelength and strike length than the antiforms to the north.

Although dominated by glacial erosion, the Hayes Range appears to defy the glacial buzzsaw operating over the rest of the Alaska Range: it is high, but not as high as the "Teflon peaks" of the Denali massif. The Hayes Range is intermediate between these two extremes, with high uplift rates compensating for more erodible rock types. Topography in the Hayes Range exceeds what would be expected if glacial erosion kept pace with rock uplift. The Teflon peaks argument is not sufficient to explain the high topography. A major young antiform in the Hayes Range can account for the rapid rock uplift needed. Erosion is outpacing rock uplift in the narrow backlimb of this antiform, but incision has allowed the preservation of high peaks and ridgelines across its wide crest and forelimb.

I hope that the identification and description of the elliptical Hayes Range antiform contributes to an emerging understanding of the complex neotectonics of a dynamic and relatively little-studied part of the Alaska Range. Crossing the transition from well-defined Quaternary structures that have not been obscured by glaciation into progressively more glaciated terrain provides new insight into the

complex interactions between tectonics and glaciation in the formation of topography.

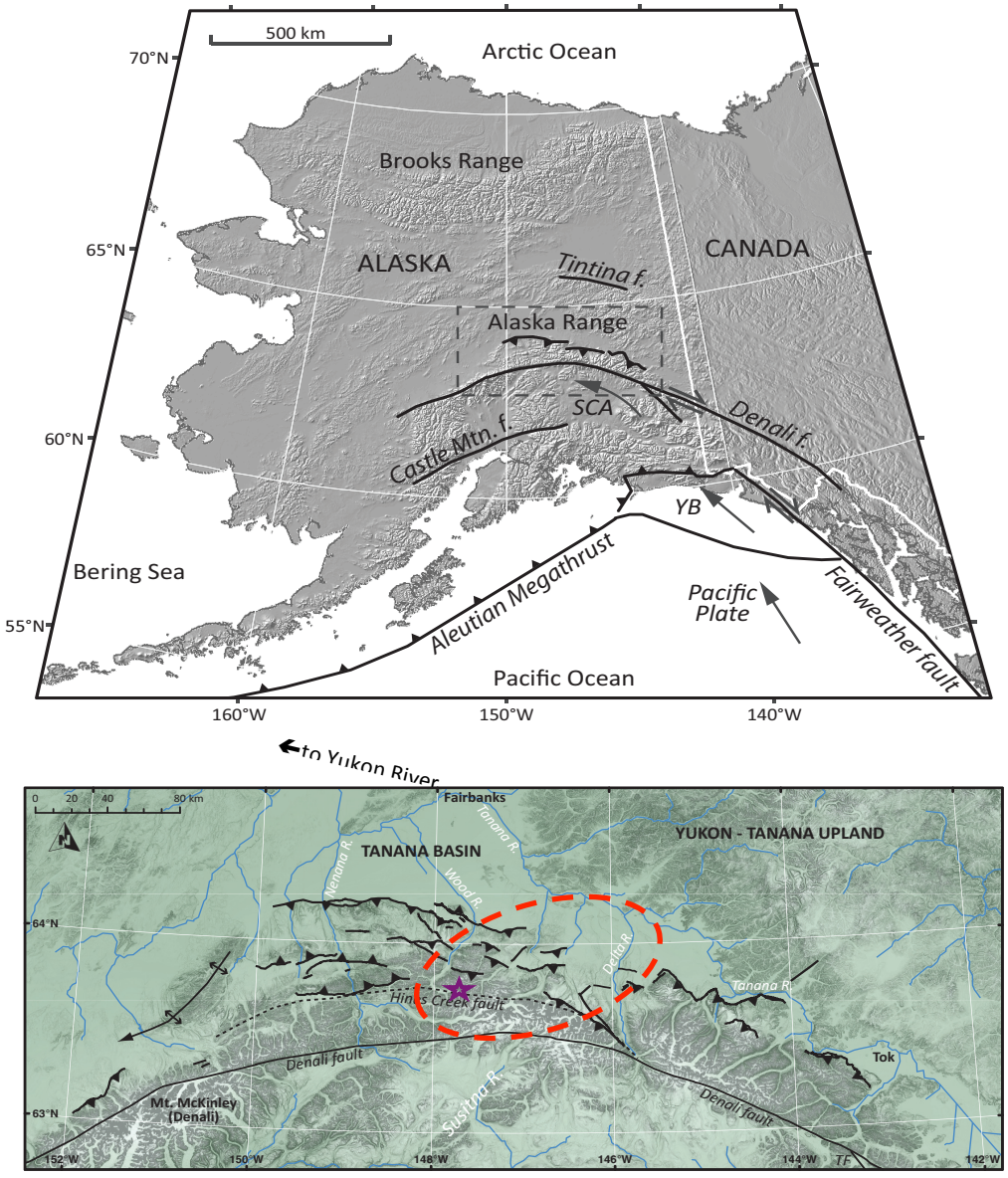

Figure 1. Tectonic setting of the Alaska Range including the Yakutat Block (YB) and the portion of south-central Alaska adjacent to the Denali fault system (SCA)(top). Hayes Range study area between Wood and Delta Rivers (bottom, red ellipse), and Anderson Mountain field site (bottom, purple star). Modified from Bemis et al., 2012.

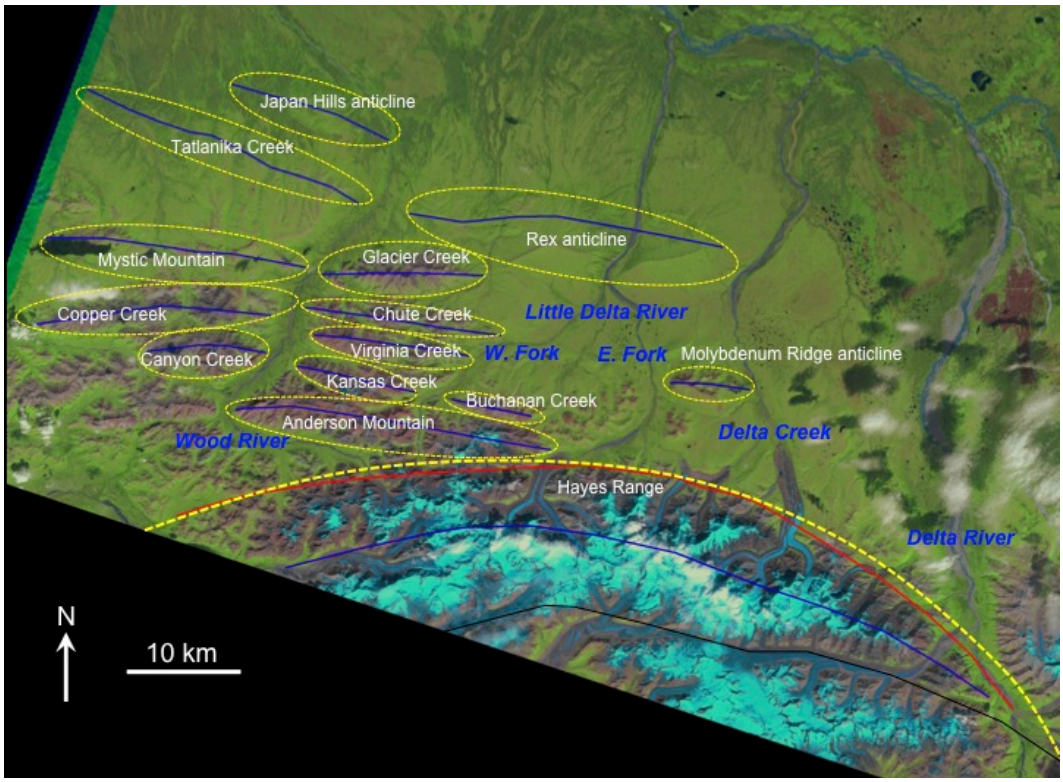

Figure 2. Regional topography of the Hayes Range and its foothills between the Wood and Delta Rivers shows a series of elliptical highs (outlined in yellow) trending WNW-ESE, around which glacial and river valleys are diverted, e.g., the Wood and Little Delta Rivers in the center of the image. Blue lines indicate hypothesized antiform hinges. Names assigned by Bemis et al. (2012) are followed by "anticline"; antiforms identified in this study are identified by names of nearby geographic features. Denali fault trace shown in black. Landsat 7 natural color composite, modified by author.

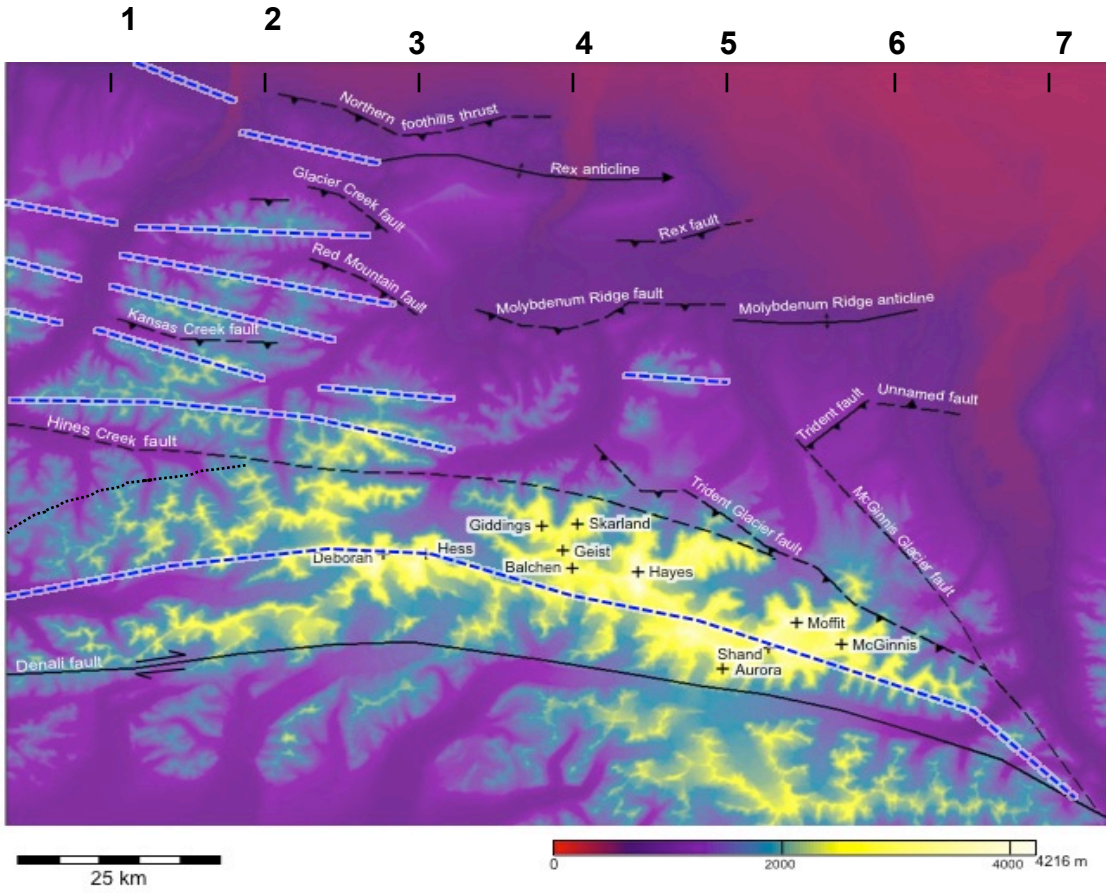

Figure 3. Hayes Range structural features and named summits superimposed on regional DEM (faults from Bemis et al., 2012; 10 m DEM courtesy of Casey Denny, GINA). Numbers at top mark the north end of sections shown in Figure 5. Dashed blue lines show approximate locations of inferred antiform hinges. Dotted black line shows the inferred thrust fault along the northwestern boundary of the Hayes Range antiform.

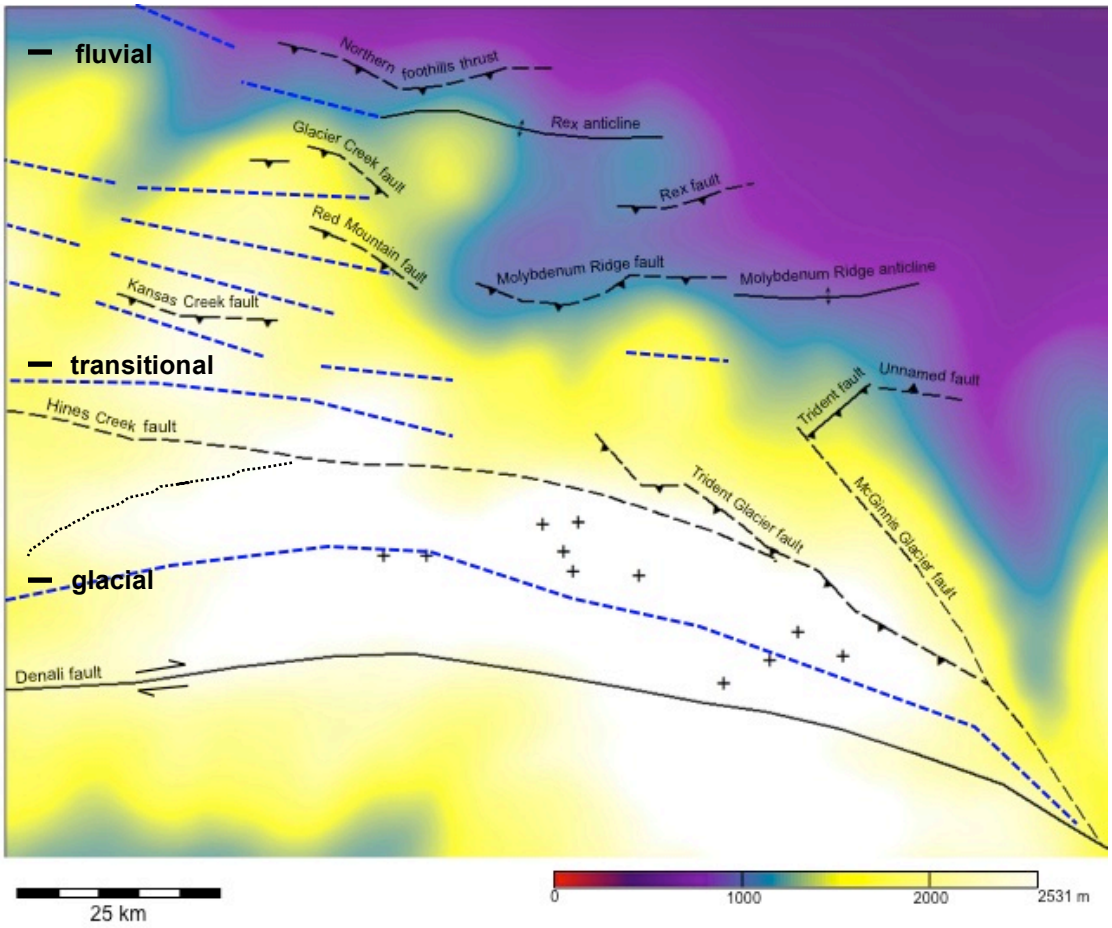

Figure 4. Map of mean elevation with selected major structural and topographic elements from Figure 3 shown for reference. Dashed blue lines show approximate locations of inferred antiform hinges. Dotted black line shows the inferred thrust along the northern boundary of the Hayes Range antiform. Profile lines for fluvial, transitional, and glacial zone mean elevation profiles shown along left side.

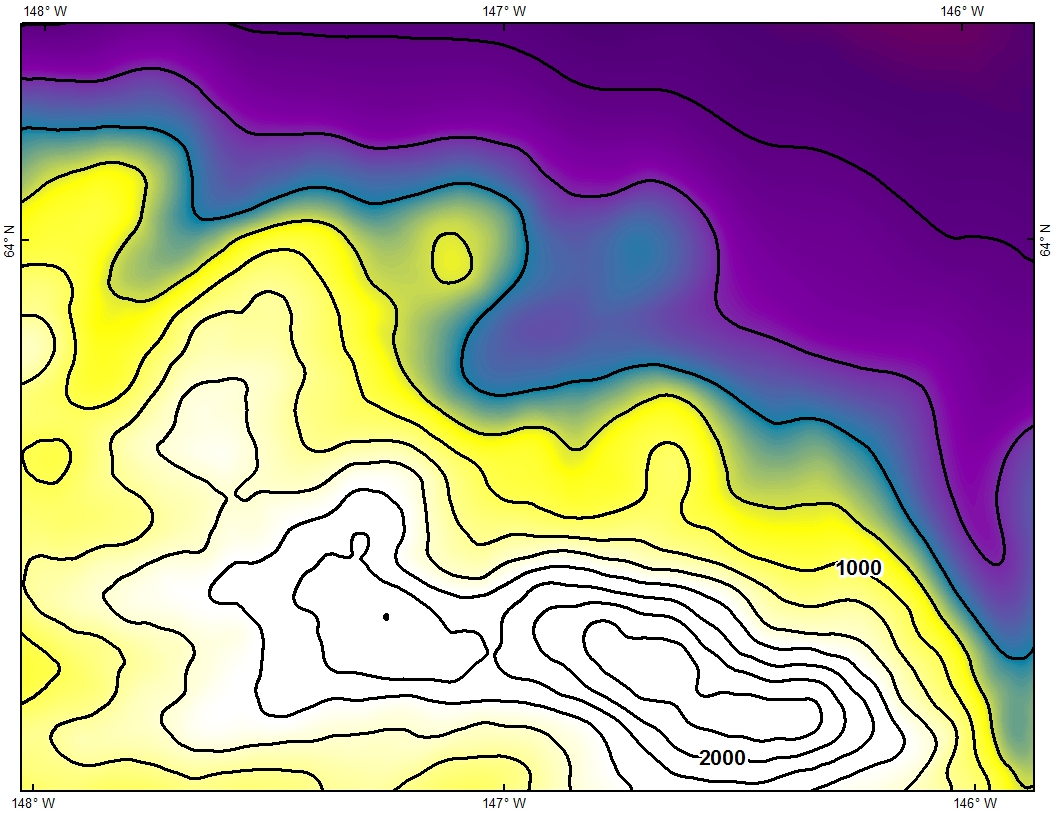

Figure 5. Map of mean elevation with 200 m contours shown.

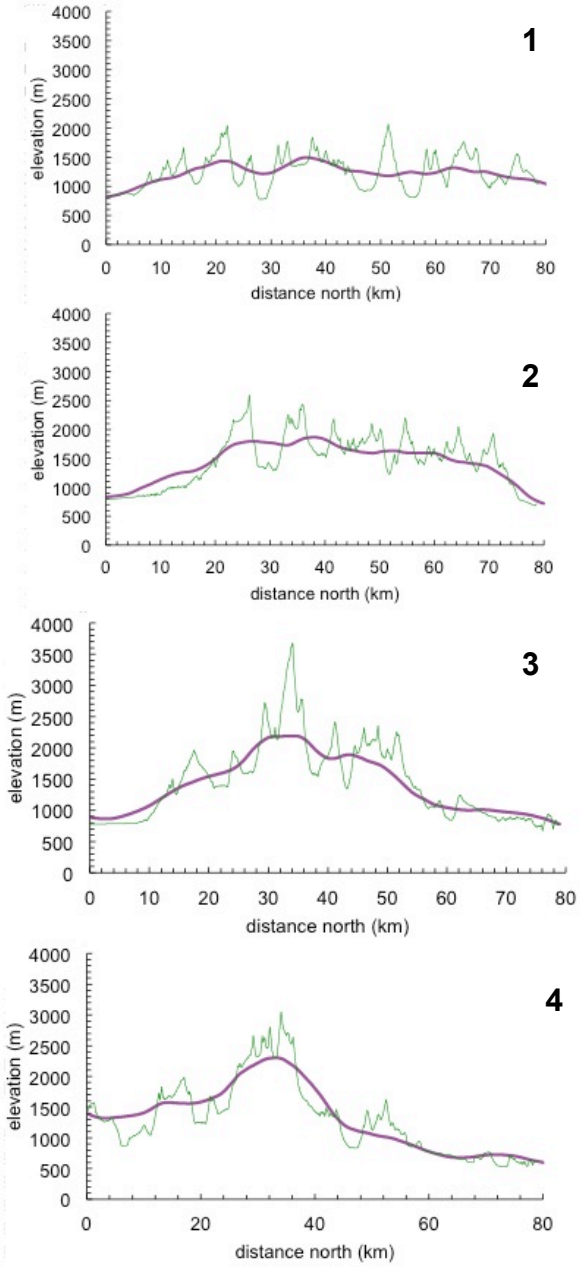

Figure 6. South-north topographic profiles across the Hayes Range topographic high, from west (1) to east (4), spaced ~20 km apart; Figure 3 shows location of profile lines. Green profiles extracted from DEM, purple from mean elevation map. 16× vertical exaggeration.

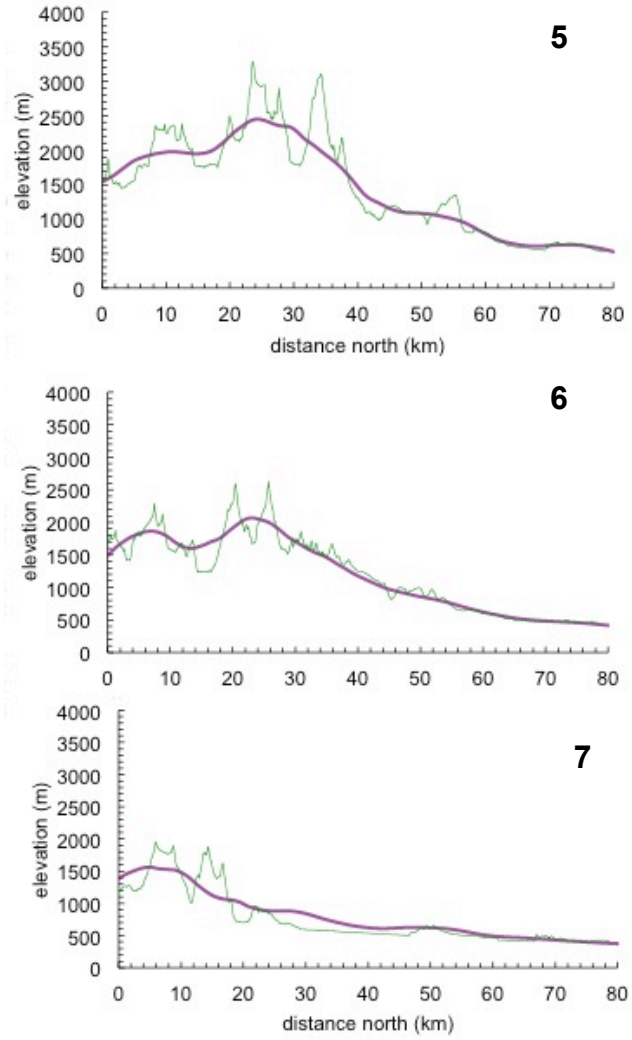

Figure 7. South-north topographic profiles across the Hayes Range topographic high, from west (5) to east (7), spaced ~20 km apart; Figure 3 shows location of profile lines. Green profiles extracted from DEM, purple from mean elevation map. 16× vertical exaggeration.

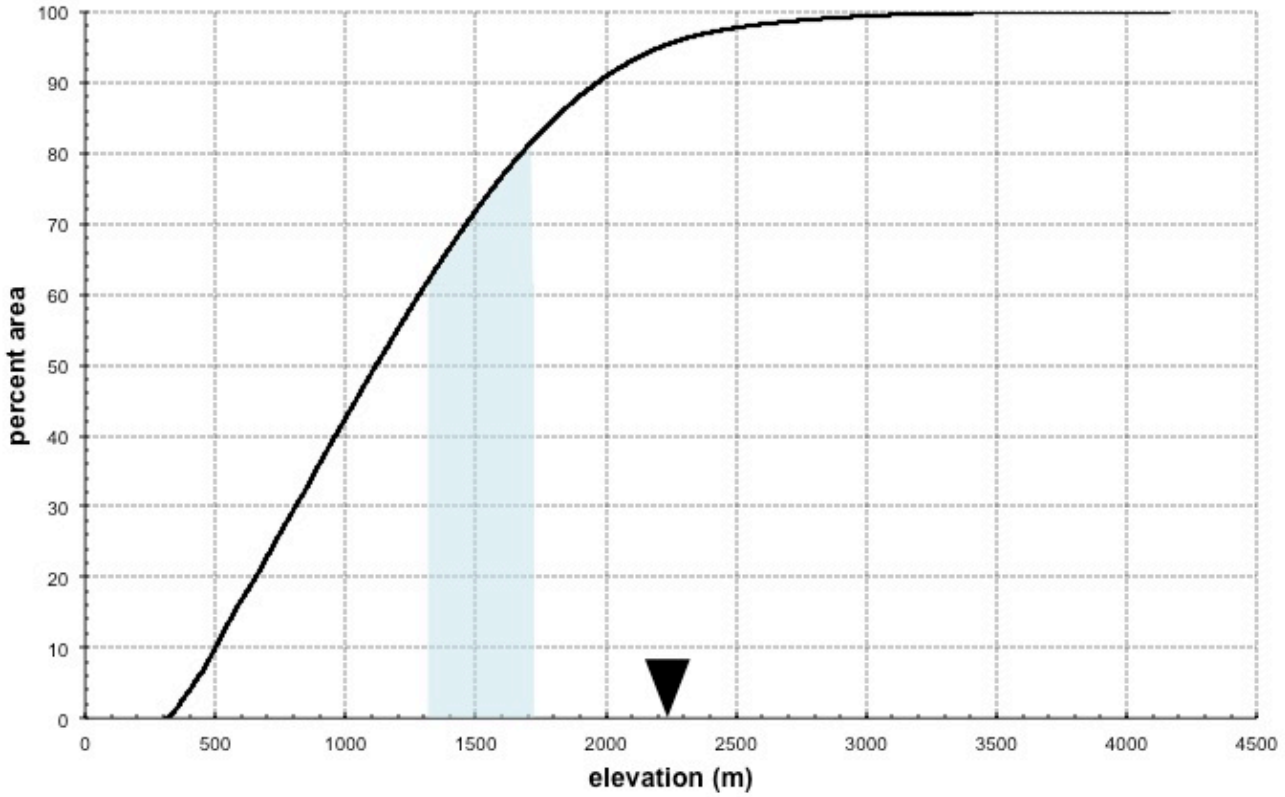

Figure 8. Hypsometric curve for the Hayes Range study area. Dark triangle indicates mean elevation (2235 m); blue shading shows altitudinal range of the modern equilibrium line altitude (ELA) calculated using the accumulation area ratio (AAR) (1320-1710 m).

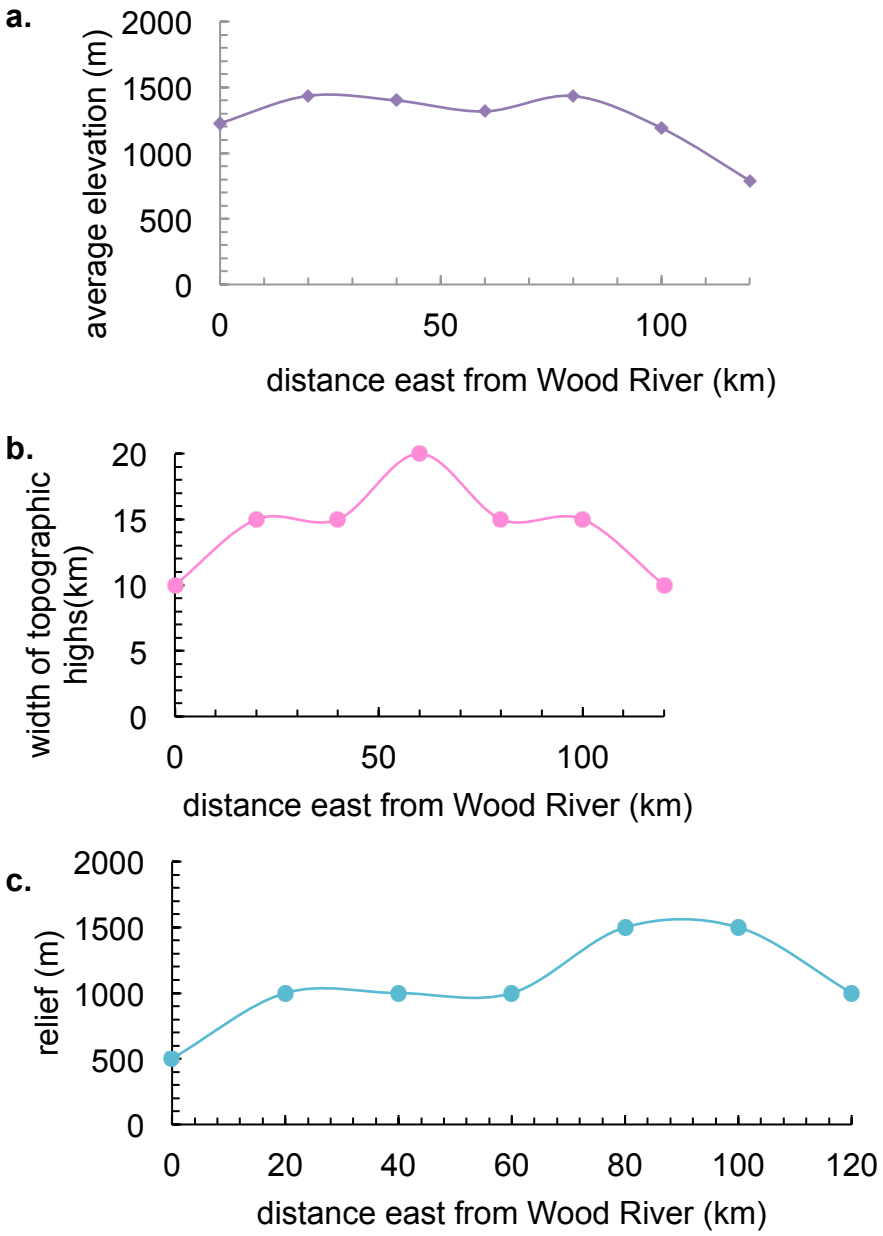

Figure 9. Elevation, width, and relief. (a) Variation in Hayes Range mean elevation values from west to east for profiles 1-7 (Fig. 3); 34 × vertical exaggeration. (b) Variation in average width of topographic highs from west to east. (c) Variation in average relief from west to east; 34 × vertical exaggeration.

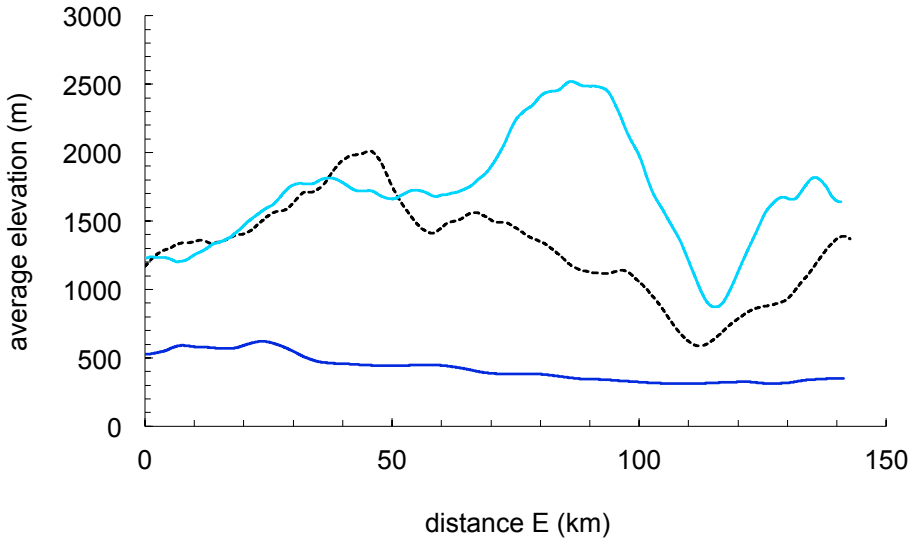

Figure 10. Zonal variation in Hayes Range mean elevation values from west to east;, see Figure 4 for profile lines across zones of predominantly fluvial (dark blue) and glacial (light blue) erosion, as well as a transitional zone (dotted black); 34 × vertical exaggeration.

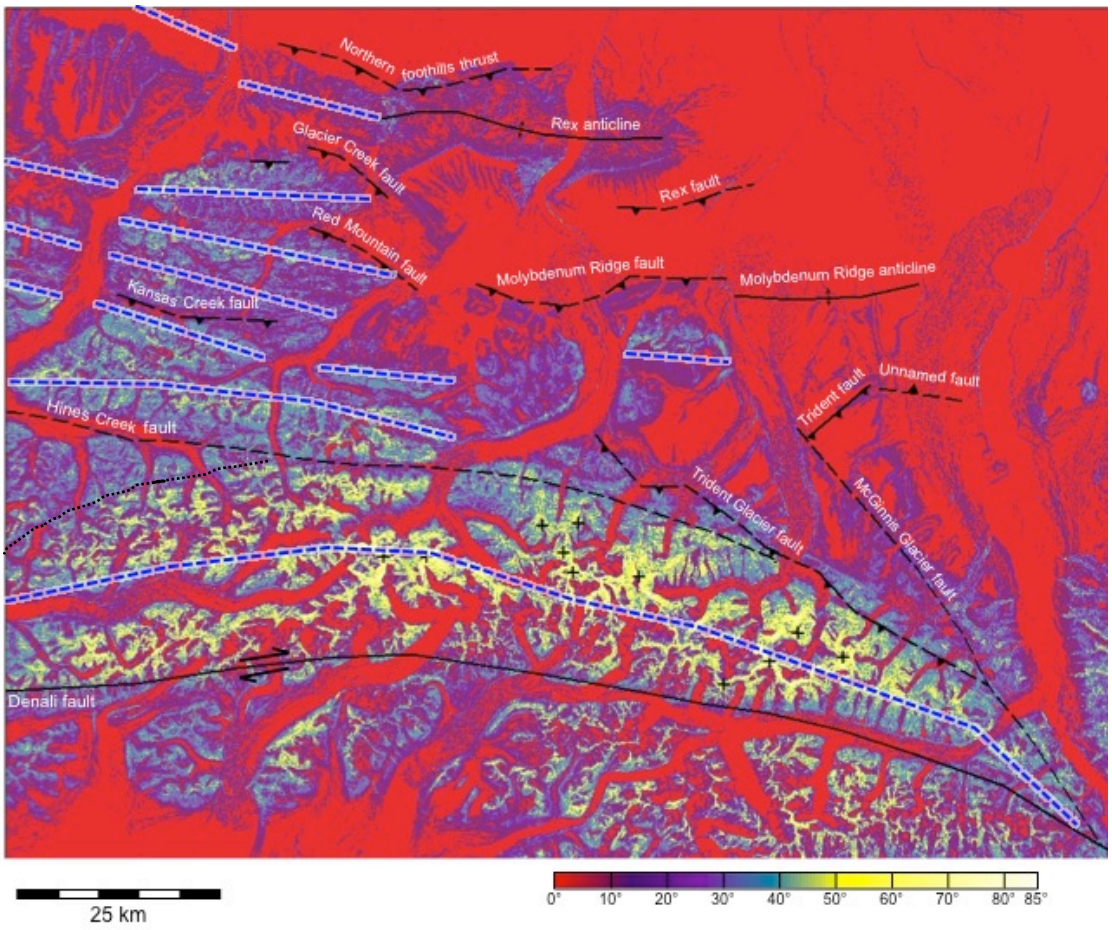

Figure 11. Slope map. Blue dashed lines indicate antiform hinges. Dotted black line shows the inferred thrust along the northern boundary of the Hayes Range antiform.

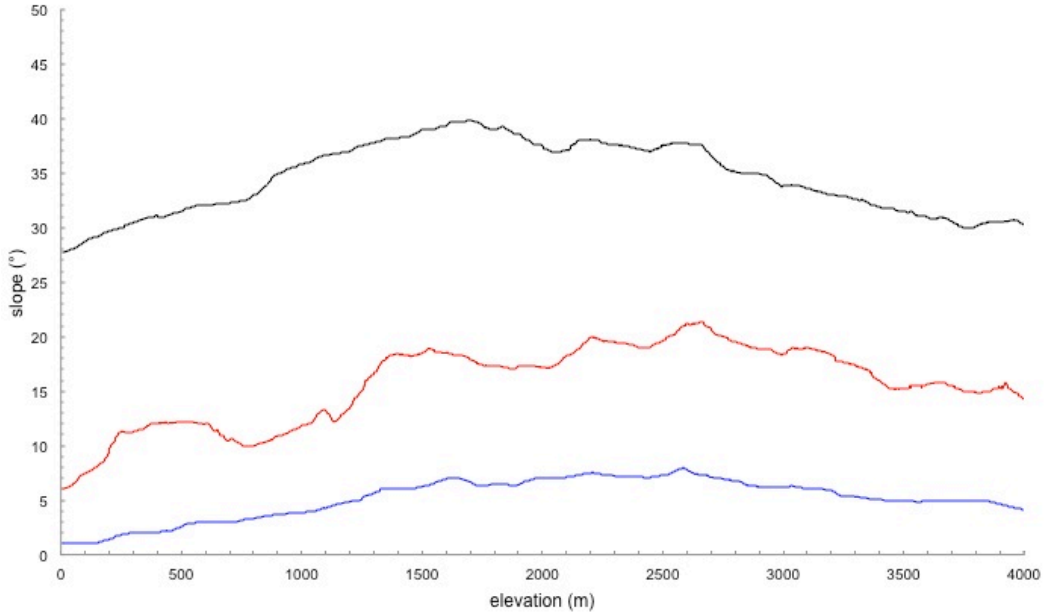

Figure 12. Slope/altitude distribution for the Hayes Range (at right). Graph shows the 25th , 50th and 75th percentiles of slope distribution (blue, red, and black, respectively).

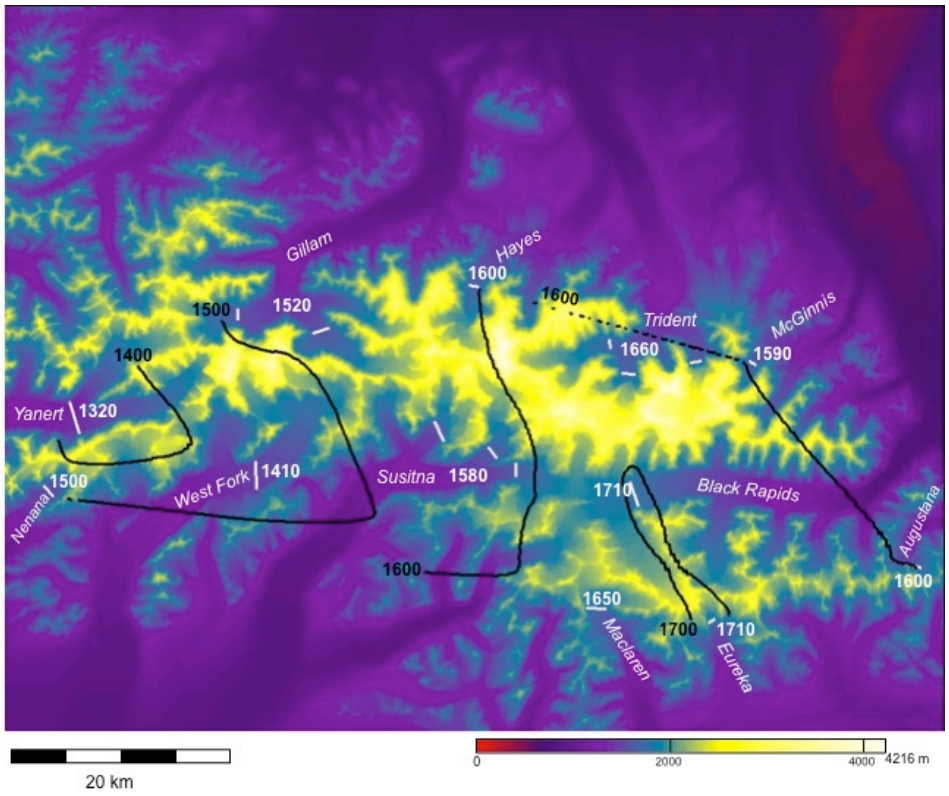

Figure 13. Contours of modern AAR ELA shown in black; approximate ELA locations and values shown in white. Glacier inventory data from Arendt et al. (2013).

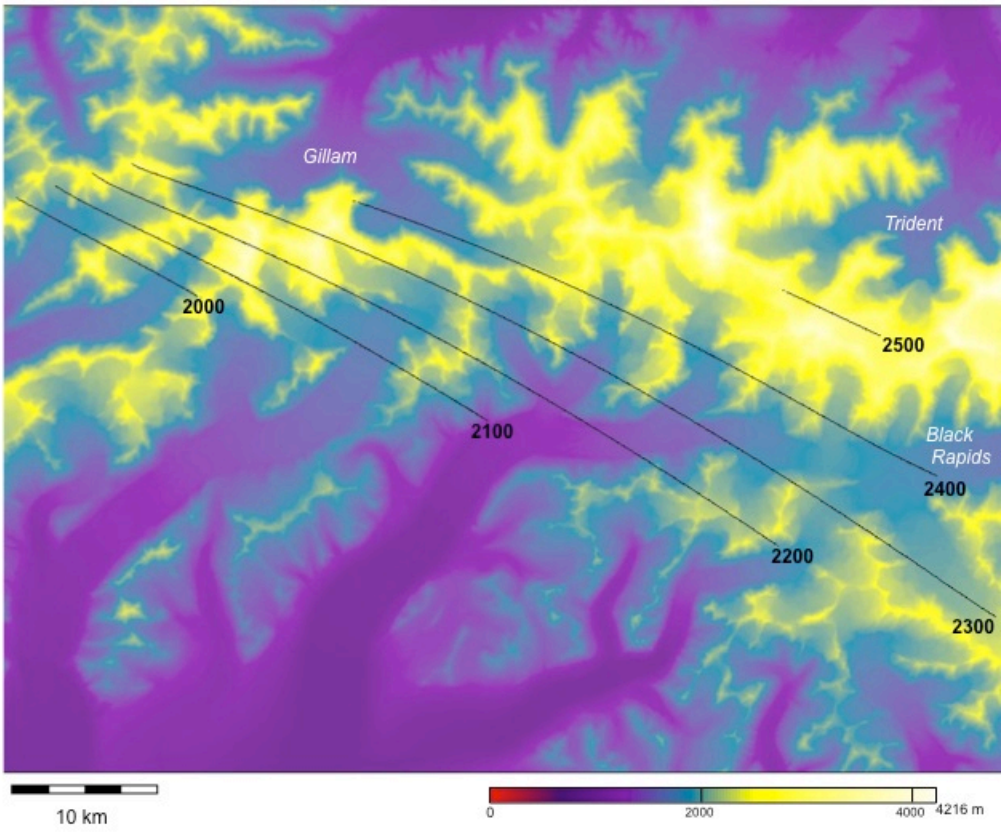

Figure 14. Contours of modern toe-summit altitude method (TSAM) ELA. LGM moraines are clearly identifiable only for the Gillam, Trident, and Black Rapids glacier complexes, so these are the only TSAM ELAs that were compared.

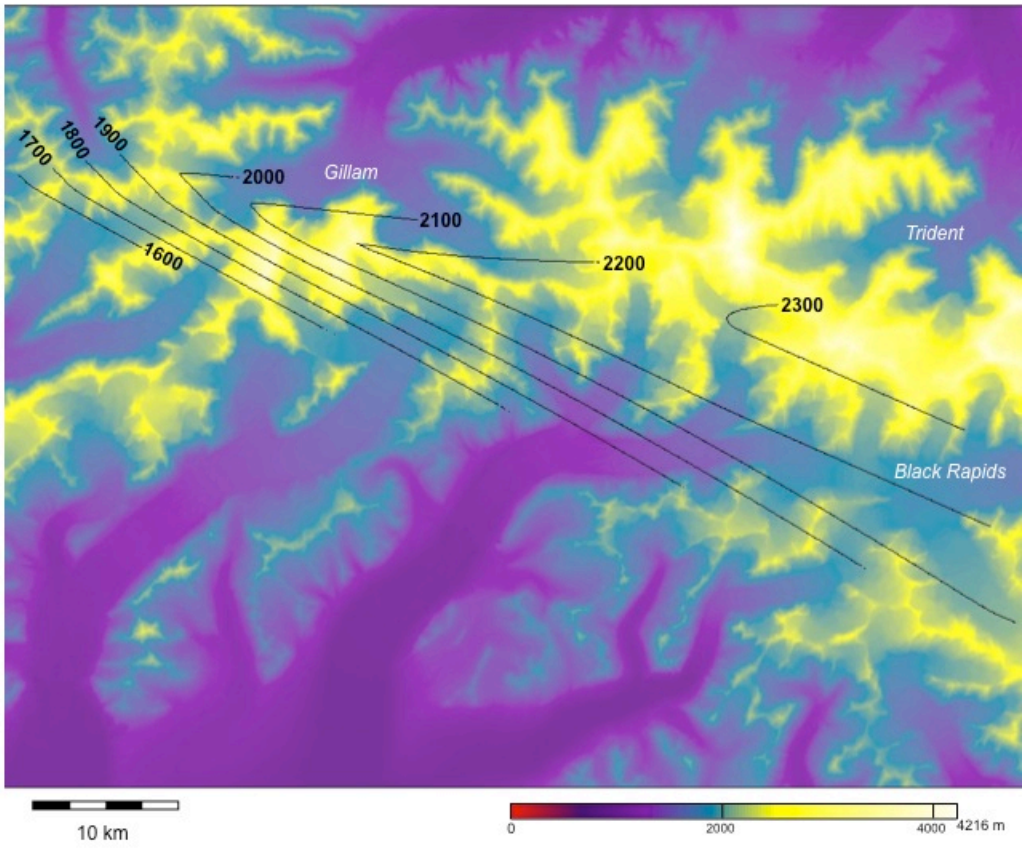

Figure 15. Contours of last glacial maximum (LGM) TSAM ELA. LGM moraines are clearly identifiable only for the Gillam, Trident, and Black Rapids glacier complexes, so these are the only TSAM ELAs that were compared.

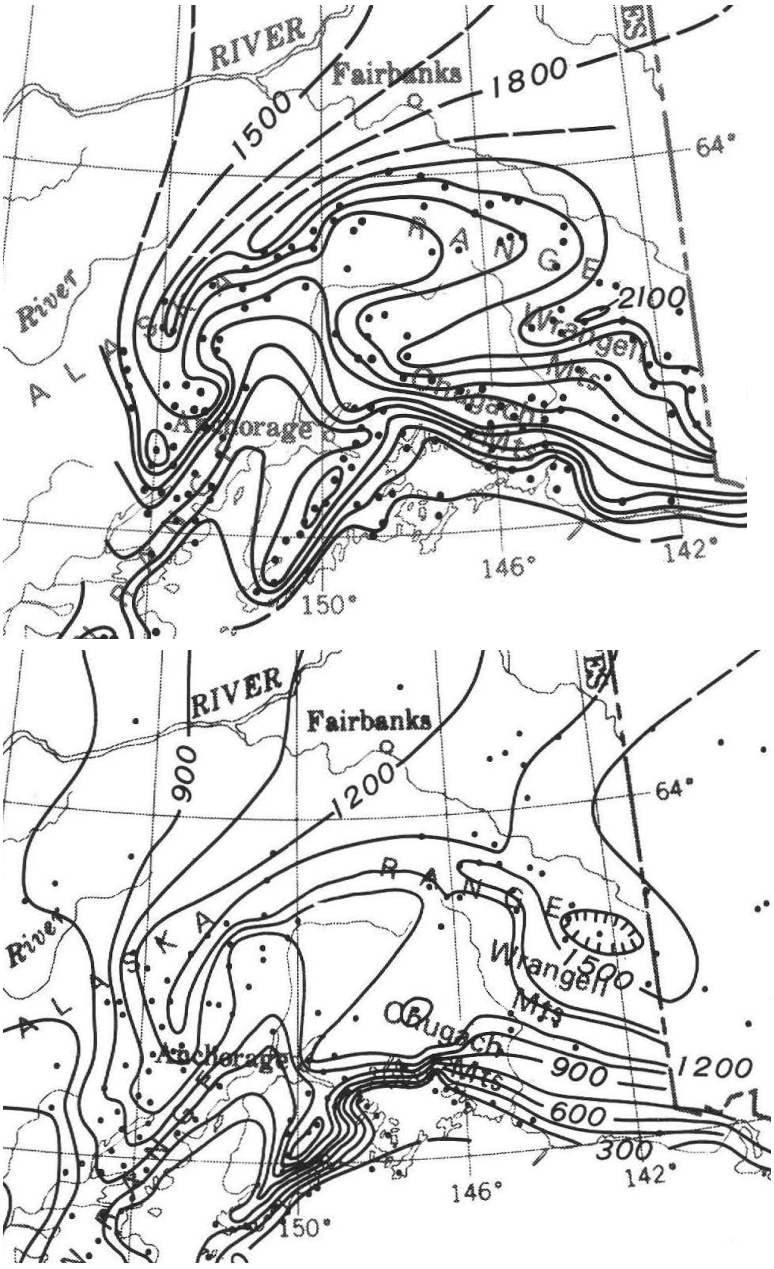

Figure 16. Contours of modern (top) and LGM ELA for the Chugach Mountains, Alaska Range, and Yukon-Tanana upland, modified from Péwé (1975).

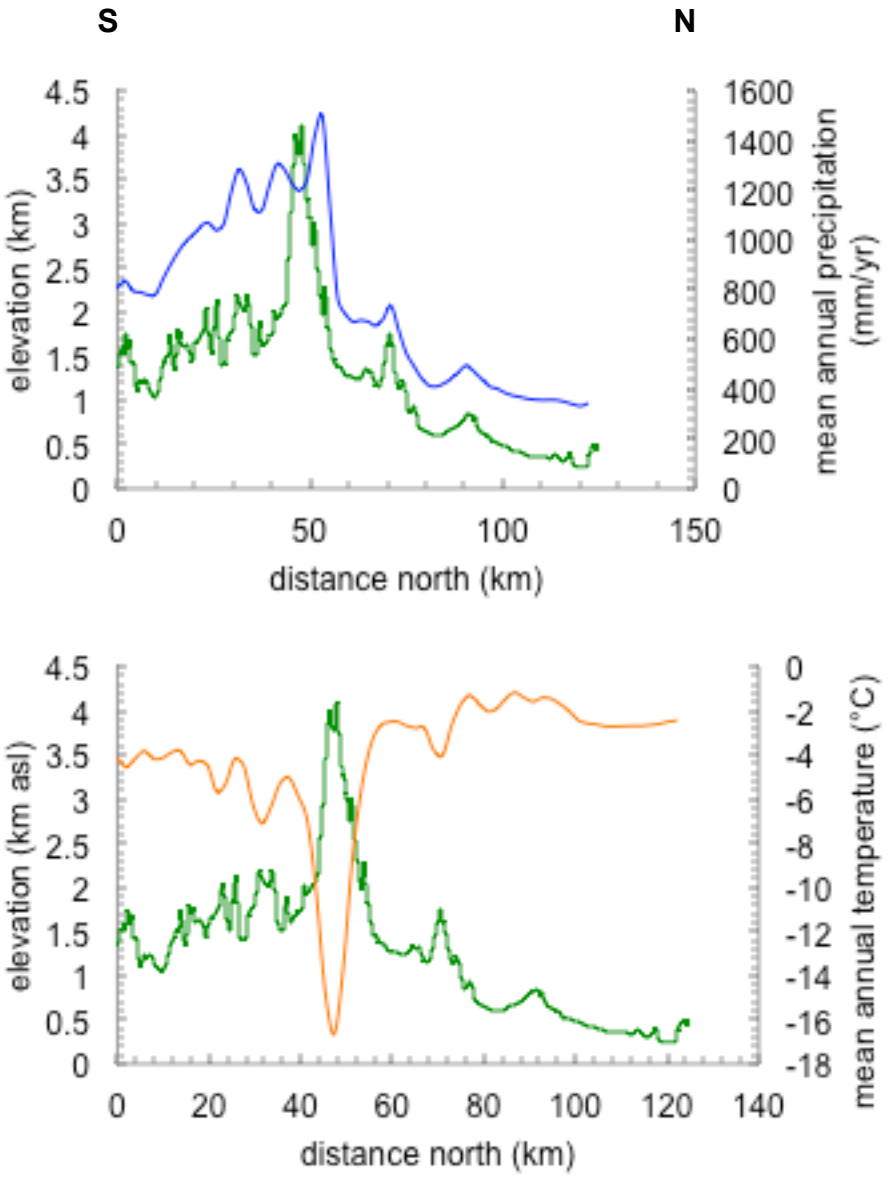

Figure 17. Regional precipitation (top, blue line) and temperature (bottom, orange line) gradients across the Hayes Range, S-N. Green topographic profiles extracted from DEM. Line of section shown on Figure 13. PRISM climate data from Daly et al., (1994). 33× vertical exaggeration.

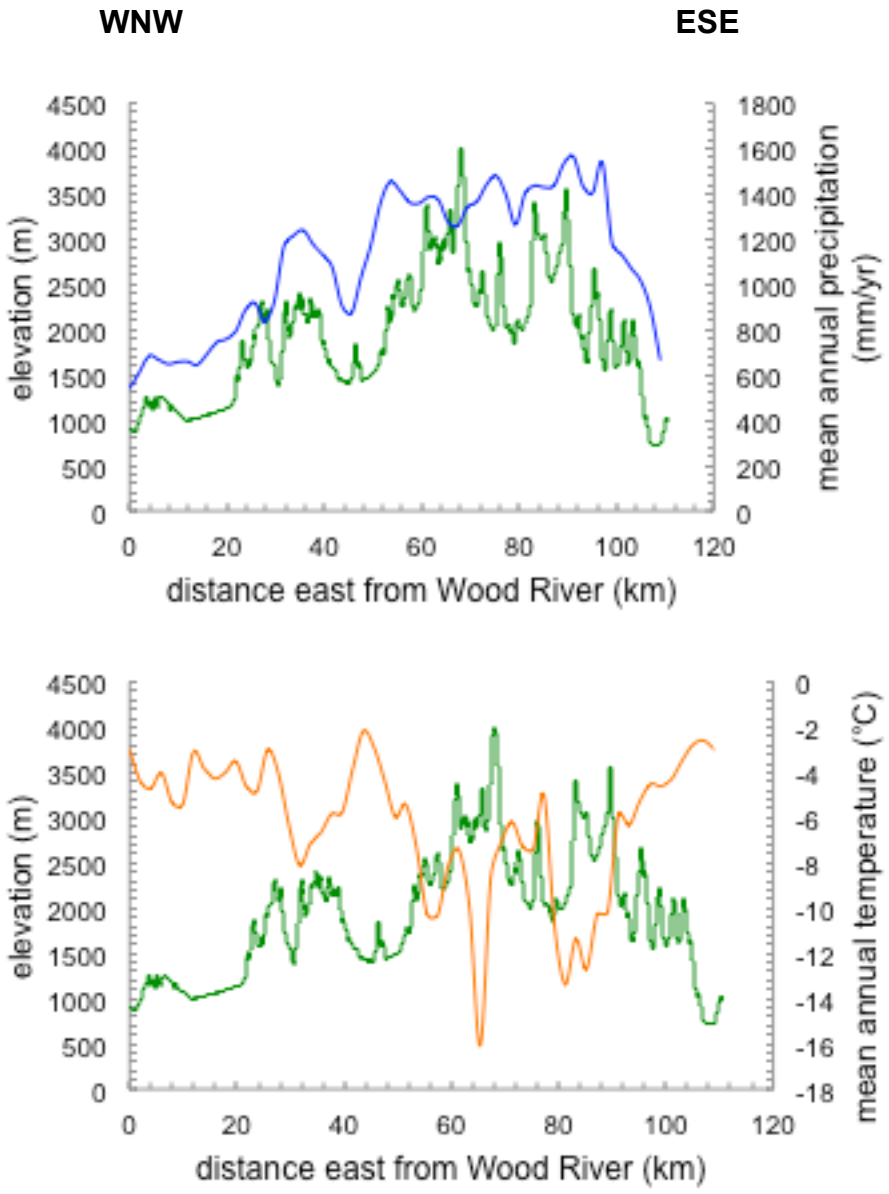

Figure 18. Regional precipitation (top, blue line) and temperature (bottom, orange line) gradients across the Hayes Range, W-E. Green topographic profiles extracted from DEM. Line of section shown on Figure 13. PRISM climate data from Daly et al., (1994). 33× vertical exaggeration.

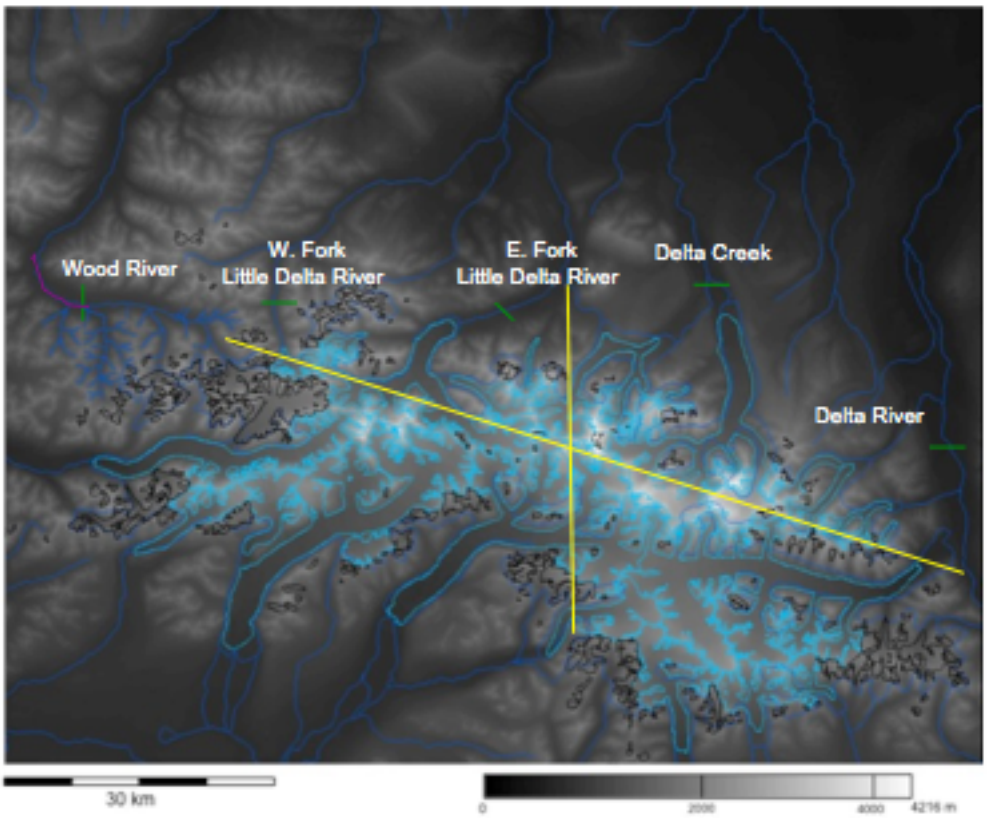

Figure 19. Extent of modern glaciers and rivers in Hayes Range. Streams are dark blue; valley glaciers are outlined in light blue and alpine glaciers in black. Glacial extents from Arendt et al. (2013); streams, state hydrology layer, courtesy of GINA. Climate profile lines (Fig. 17, 18) shown in yellow, valley cross-section lines (Fig. 22, 24-26) in green, and GPS longitudinal profile line in purple (Fig. 23).

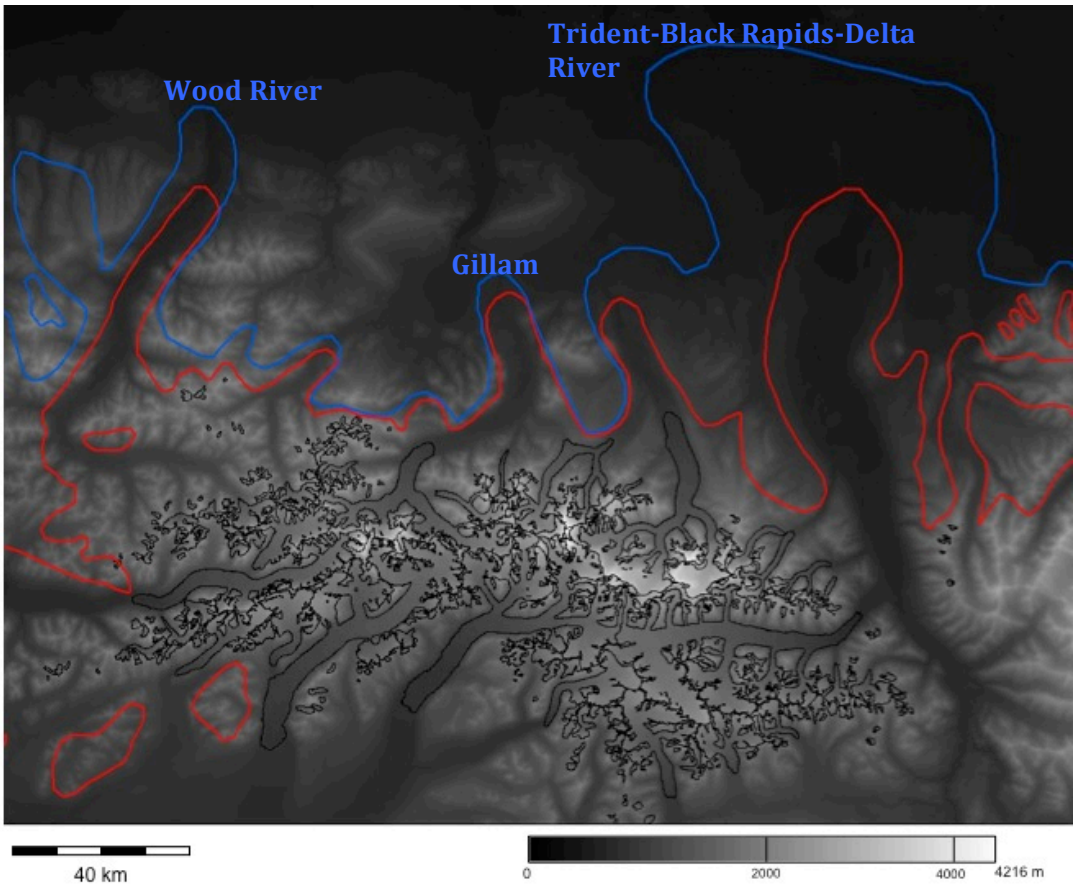

Figure 20. Previous extent of glaciers in Hayes Range: modern (black), Late Wisconsin (red), and maximum (blue) (Manley and Kaufman, 2002). Glacier complexes identified labeled in blue.

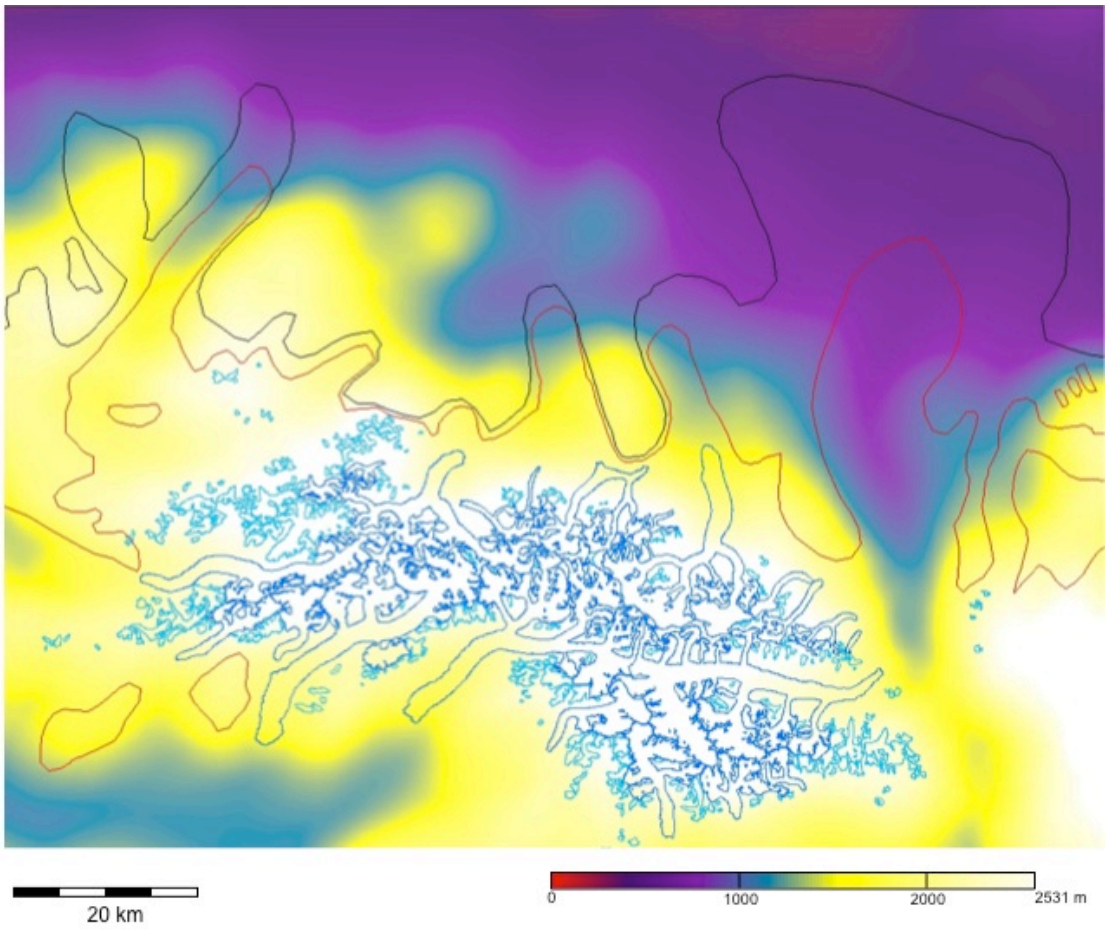

Figure 21. Extent of glaciers vs. mean elevation in the Hayes Range. Modern alpine glaciers are outlined in light blue, and valley glaciers in dark blue. Extent of Late Wisconsin glaciers outlined in red, extent at maximum in black (Manley and Kaufman, 2002).

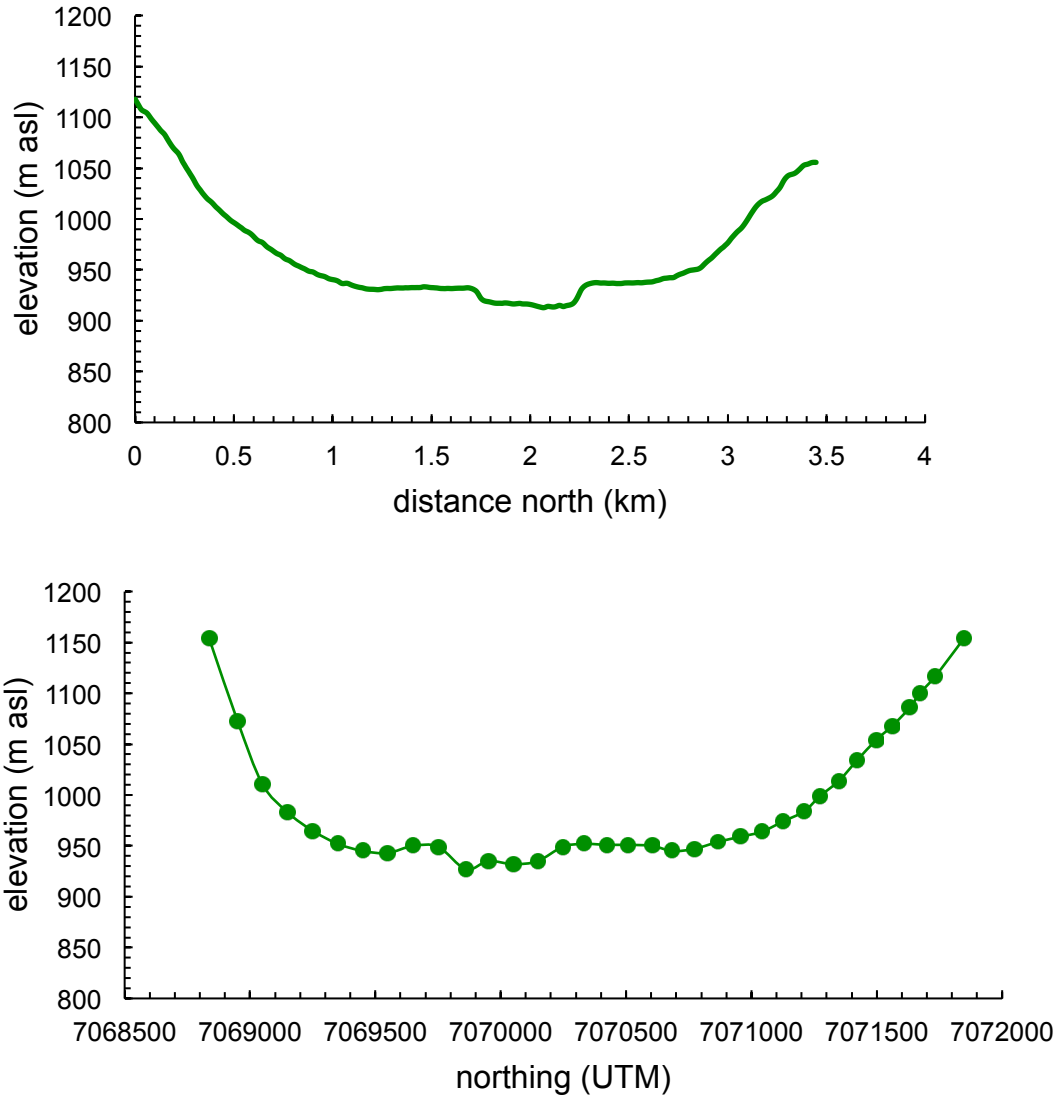

Figure 22. Wood River cross-valley profiles extracted from 10 m DEM (top) and based on GPS waypoints from fieldwork (bottom). 30× vertical exaggeration. Profile lines shown on Figure 13.

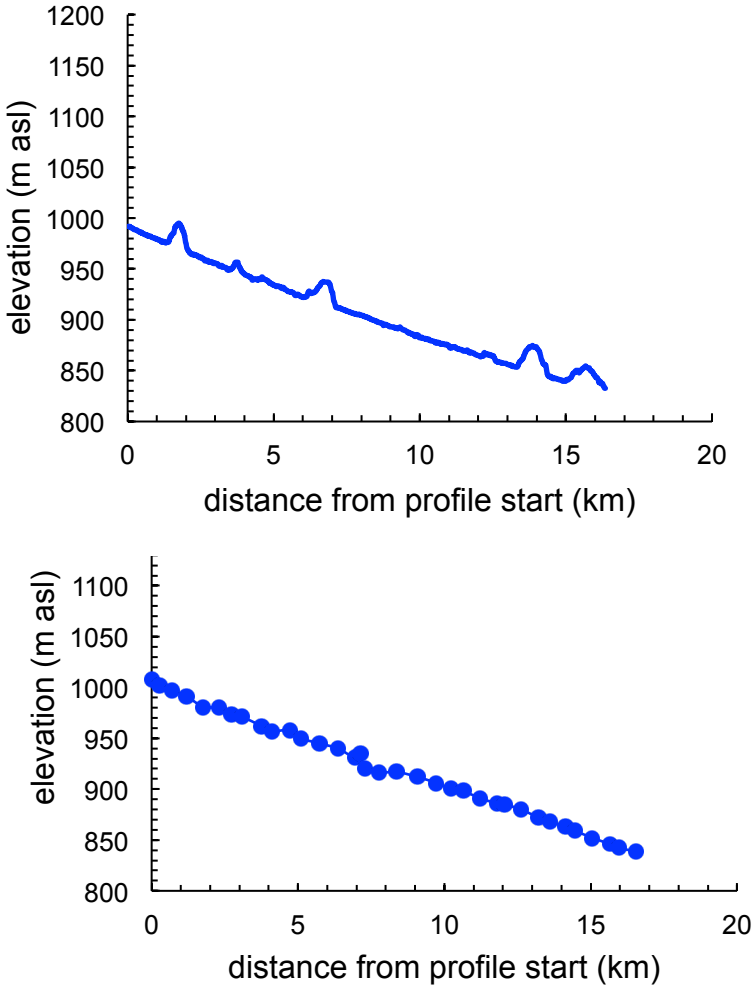

Figure 23. Longitudinal profiles for a segment of the Wood River extracted from 10 m DEM (top) and based on GPS waypoints from fieldwork (bottom). 27× vertical exaggeration. Profile line shown on Figure 13.

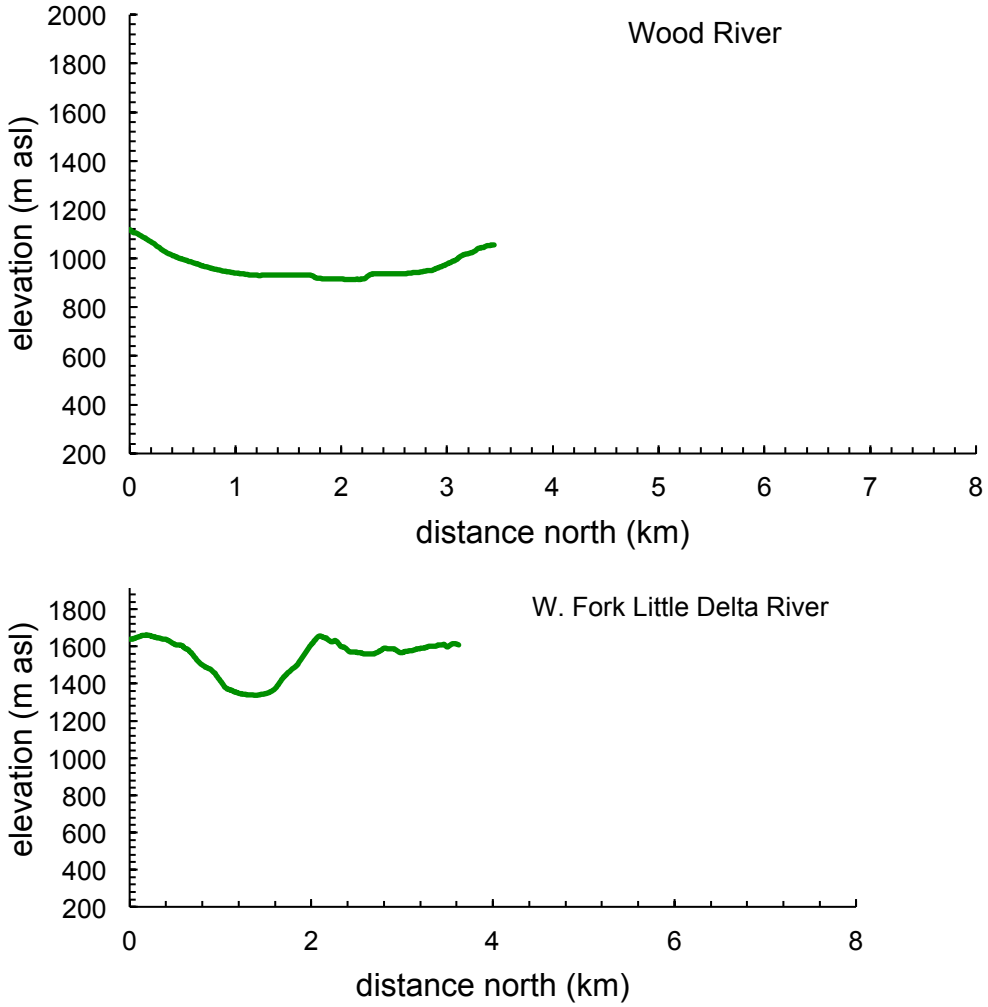

Figure 24. Cross-valley profiles of major drainages in Hayes Range study area, extracted from 10 m DEM. 2× vertical exaggeration. Profile lines shown on Figure 13.

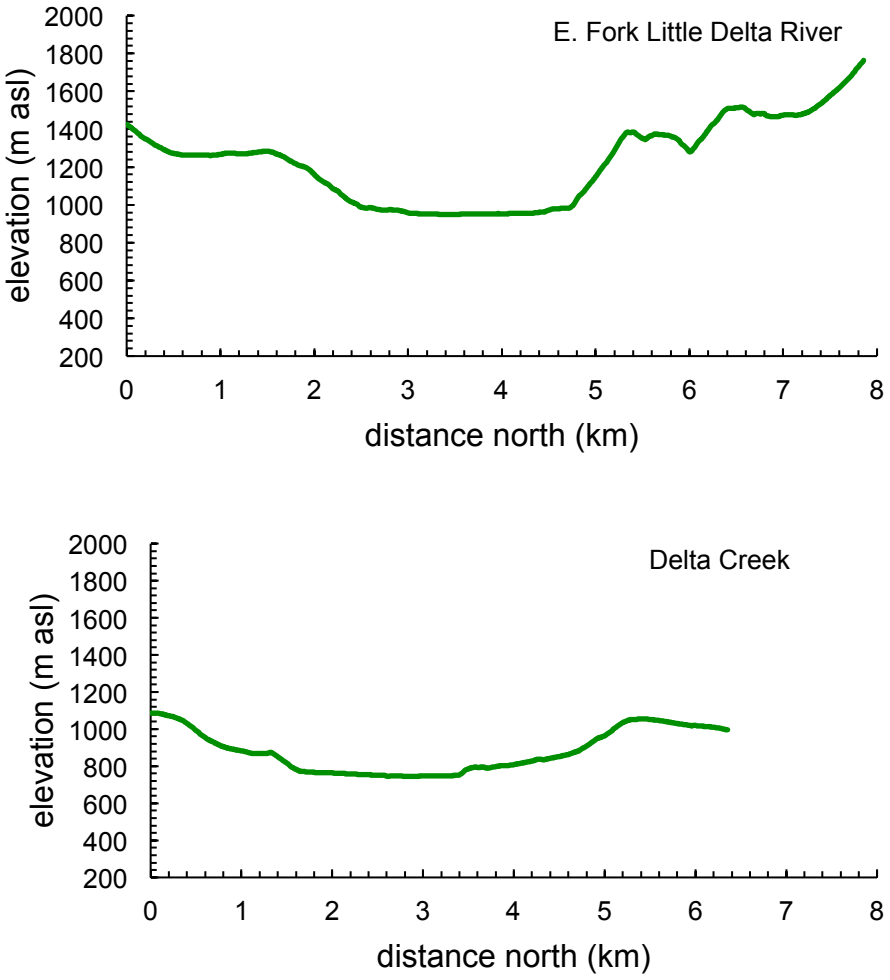

Figure 25. Cross-valley profiles of major drainages in Hayes Range study area, extracted from 10 m DEM. 2× vertical exaggeration. Profile lines shown on Figure 13.

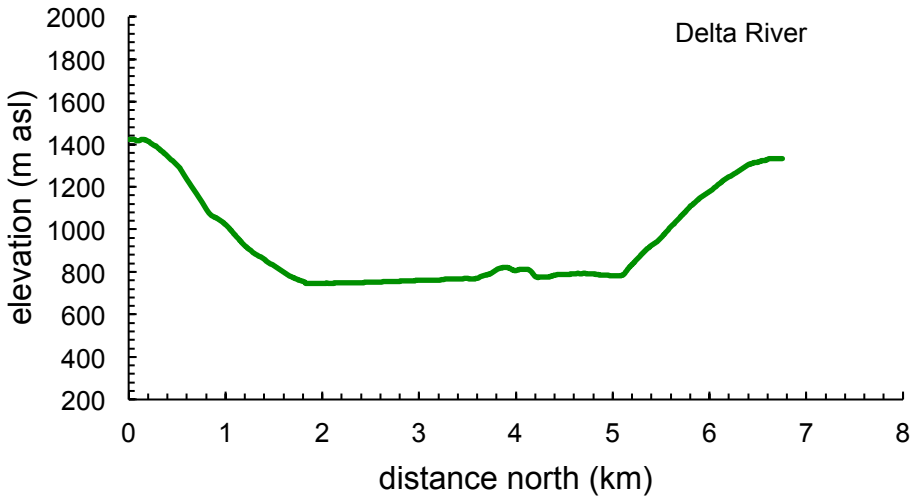

Figure 26. Cross-valley profiles of major drainages in Hayes Range study area, extracted from 10 m DEM. 2× vertical exaggeration. Profile lines shown on Figure 13.

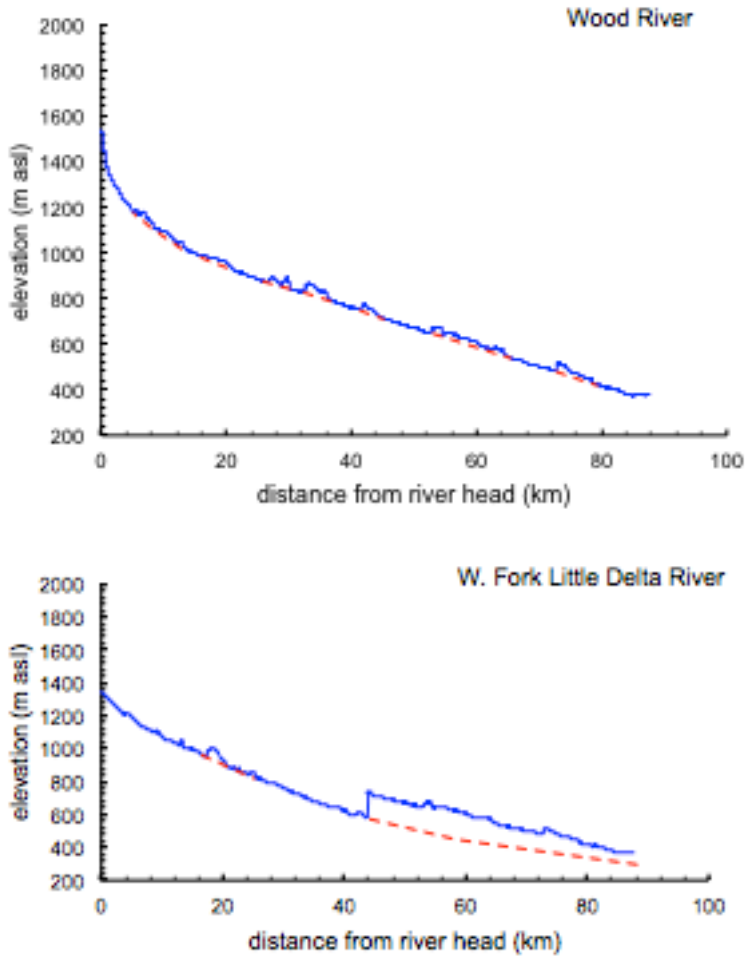

Figure 27. Longitudinal profiles, from river head to Tanana basin, of major drainages, from west to east. Dashed red lines show continuous profiles through DEM artifacts.

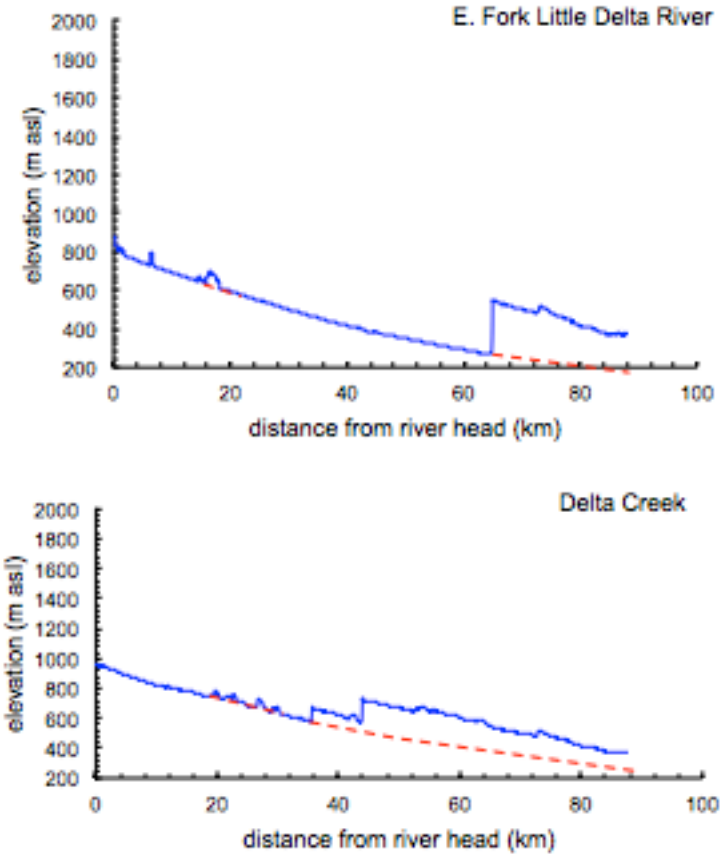

Figure 28. Longitudinal profiles, from river head to Tanana basin, of major drainages, from west to east. Dashed red lines show continuous profiles through DEM artifacts.

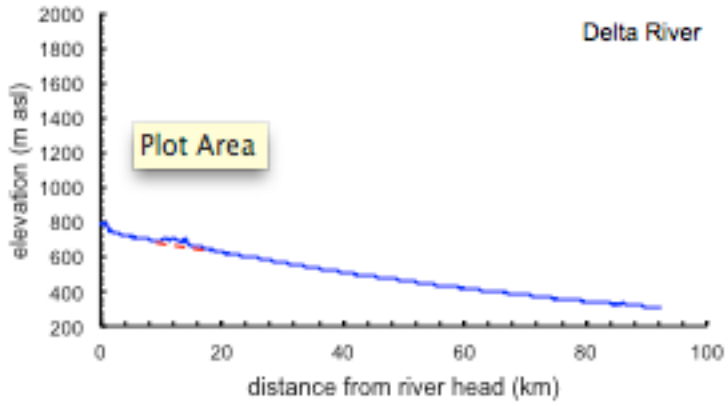

Figure 29. Longitudinal profiles, from river head to Tanana basin, of major drainages, from west to east. Dashed red lines show continuous profiles through DEM artifacts.

Figure 30. V ratios. Values used to calculate V_f and V ratios (top); values used to calculate V_c ratios (bottom). V_w = entire valley width, drainage divide to drainage divide, V_{fw} = valley floor width, A_{sc} = altitude of the stream channel, A_{rd} = altitude of right drainage divide, and A_{ld} = altitude of left drainage divide, all in meters; A_v = cross-sectional area of valley (m^2) and A_c = area of semicircle with radius equal to valley height (m^2). (Author photo of Wood River valley, Hayes Range).

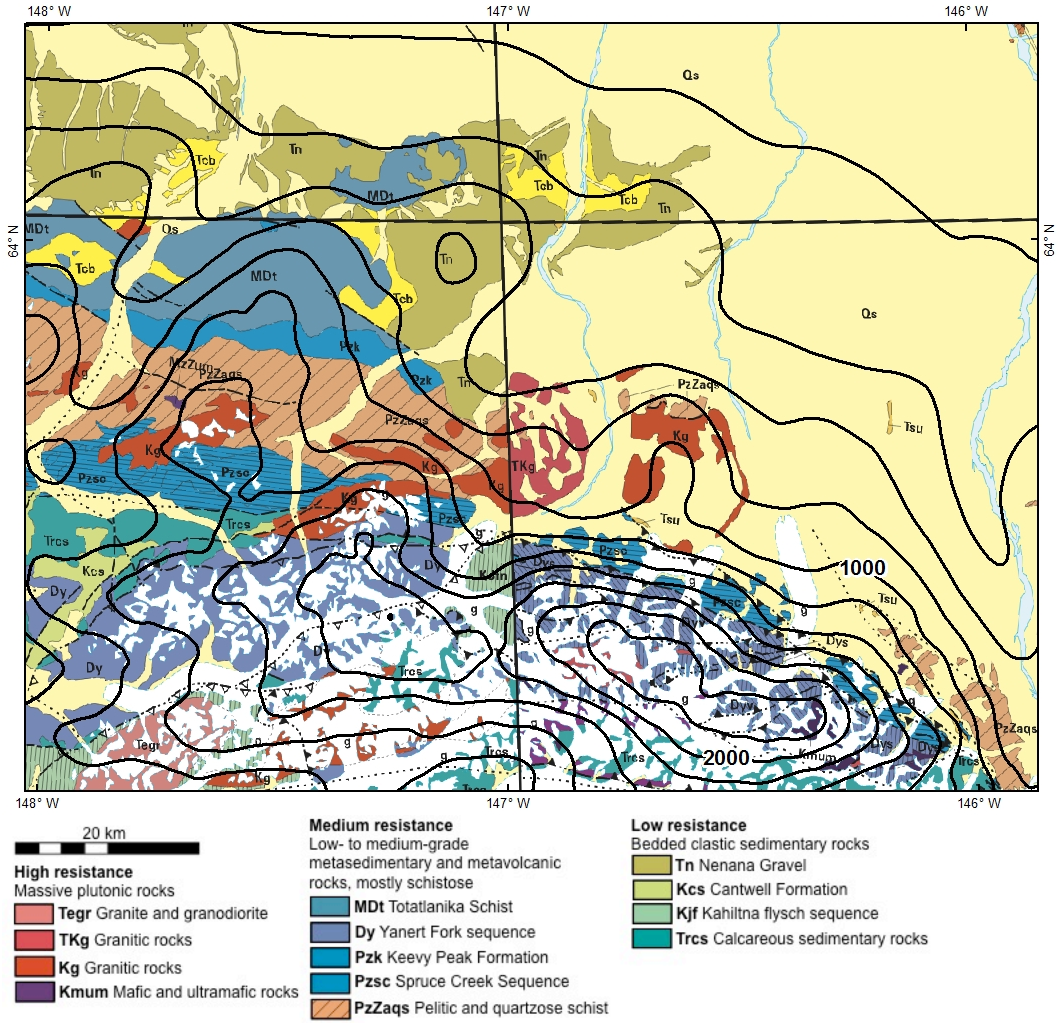

Figure 31. Map of rock type vs. mean elevation (200 m contours, shown in black). Base map from Wilson et al. (1998). See Figure 4 for mean elevation map.

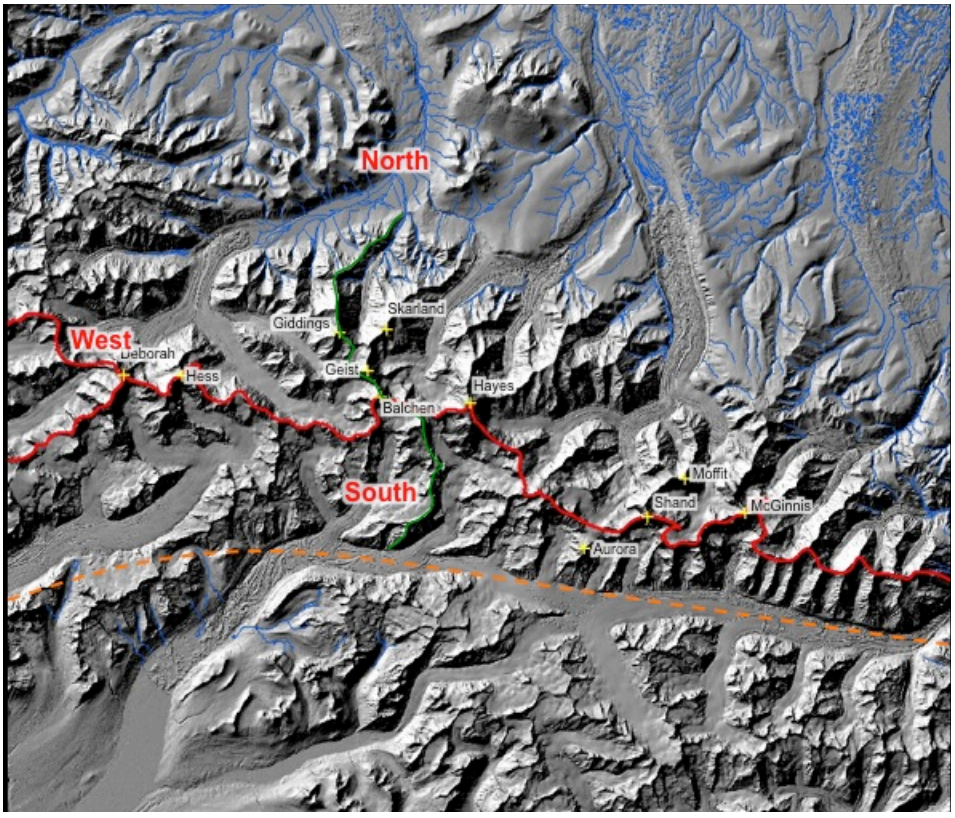

Figure 32. Drainage divides and high peaks of the Hayes Range study area. Streams shown in blue (layer courtesy of GINA). Drainage divides shown in red, and high peaks by yellow plus signs. Base map is hillshade derived from 10 m DEM (GINA). Approximate Denali fault trace shown in orange.

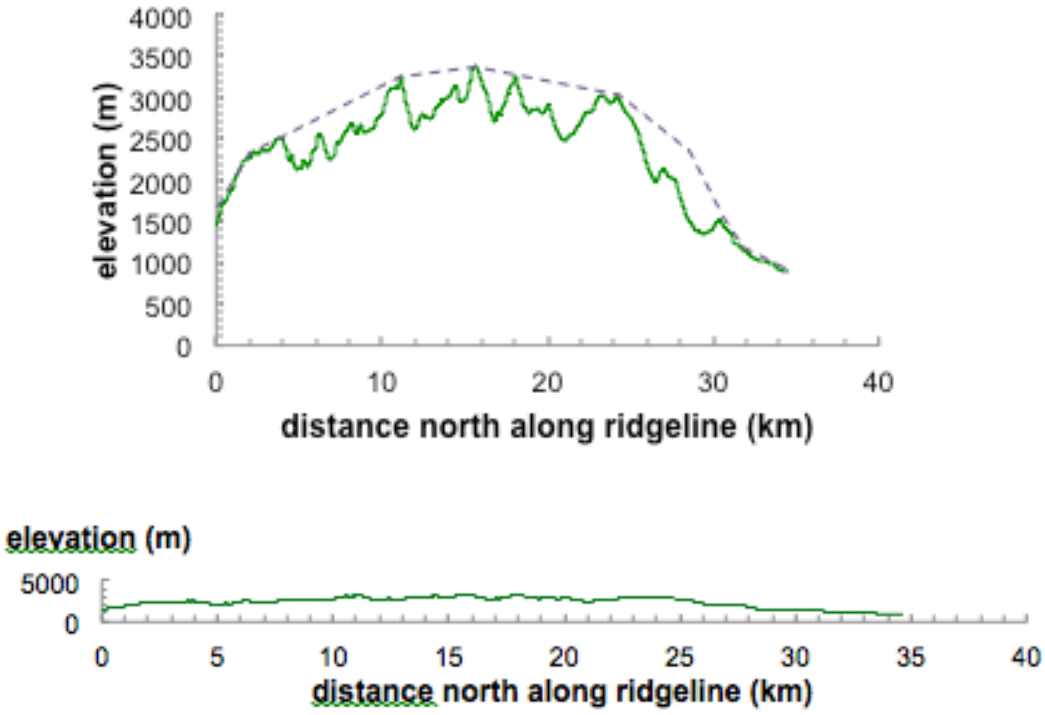

Figure 33. Ridge profile. Top: topographic profile across the inferred fold trend and along a continuous ridgeline (shown in green on Fig. 24); 34x vertical exaggeration. Distance is measured along a continuous sinuous ridgeline, so this only approximates a true profile on a plane normal to fold trend. Dashed envelope over the highest peaks shows what a folded paleo-erosion surface might have looked like prior to incision. Bottom: the same topographic profile with zero vertical

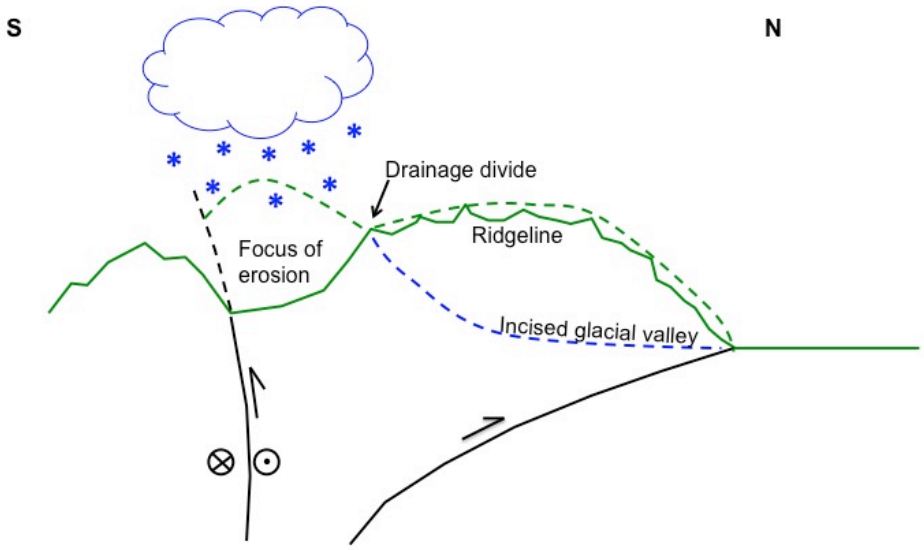

Figure 34. Tectonic interpretation cartoon shows the Hayes Range antiform, narrow, deeply incised area of focused erosion north of the Denali fault, and an incised paleosurface leading down to the range front thrust.

Table 1. Mean elevation, width, and relief for S-N profiles

Profile	Distance East from Wood River (km)	Mean		
		Elevation (m)	Width of topographic high (km)	Relief (m)
1	0	1227	10	500
2	20	1436	15	1000
3	40	1400	15	1000
4	60	1317	20	1000
5	80	1434	15	1500
6	100	1191	15	1500
7	120	790	10	1000

Table 2. Modern AAR ELAs

Glacier complex	AAR ELA (m)
Yanert	1320
West Fork	1410
Nenana	1500
Gillam	1520
Susitna	1580
McGinnis	1590
Hayes	1600
Augustana	1600
Maclaren	1650
Trident	1660
Black Rapids	1710
Eureka	1710

Table 3. Modern TSAM ELAs

Glacier complex	Toe elevation (m)	Summit elevation (m)	TSAM ELA (m)
Wood	1336	2508	1922
Little Delta	1431	2996	2214
Gillam	950	3761	2356
Trident	823	4216	2520
Black Rapids	698	3859	2279

Table 4. LGM TSAM ELAs

Glacier complex	Toe elevation (m)	Summit elevation (m)	TSAM ELA (m)
Wood	494	2508	1501
Little Delta	874	2996	1935
Gillam	630	3761	2196
Trident	568	4216	2392
Black Rapids	310	3859	2085

Table 5. Valley floor width-height (V_f) ratios

Valley	A_{sc} (m)	A_{ld} (m)	A_{rd} (m)	V_{fw} (m)	V_f	Inferred shape
Wood River	917	1117	1054	400	2.4	U
West Fork Little Delta River	1338	1660	1653	330	1.0	V
East Fork Little Delta River	949	1280	1364	2209	5.9	U
Delta Creek	745	1084	1053	1688	5.2	U
Delta River	760	1423	1332	3267	5.3	U

Table 6. Valley width-height (V) ratios

Valley	A_{sc} (m)	A_{ld} (m)	A_{rd} (m)	Valley width (m)	V
Wood River	917	1117	1054	3400	20.2
West Fork Little Delta River	1338	1660	1653	1917	6.0
East Fork Little Delta River	949	1280	1364	3869	10.4
Delta Creek	745	1084	1053	5315	16.4
Delta River	760	1423	1332	6535	10.6

Table 7. Valley semicircularity (V_c) ratios

Valley	A_v (m^2)	A_c (m^2)	Vc
Wood River	517400	62832	8.2
West Fork Little Delta River	327956	162866	2.0
East Fork Little Delta River	1005909	172098	5.8
Delta Creek	1078462	149012	7.2
Delta River	2803372	513939	5.5

Table 8. Summary of V ratios and gradient indices (k, calculated from Hack profiles)

Valley	V_f	V	V_c	k
Wood River	3.3	20.2	8.2	231
West Fork Little Delta River	1.0	6.0	2.0	193
East Fork Little Delta River	5.9	10.4	5.8	117
Delta Creek	5.2	16.4	7.2	101
Delta River	5.3	10.6	5.5	90

References

Anders, A., Mitchell, S., and Tomkin, J., 2010. Cirques, peaks, and precipitation patterns in the Swiss Alps: Connections among climate, glacial erosion, and topography. Geology 38, 239-242.

Arendt, A., Bolch, T., Cogley, J., Gardner, A., Hagen, J., Hock, R., Kaser, G., Pfeffer, W., Moholdt, G., Paul, F., et al., 2013. Randolph Glacier Inventory – A Dataset of Global Glacier Outlines: Version 3.2. Global 708 Land Ice Measurements from Space, Boulder, Colorado, USA. Digital Media.

Bates, R., and Jackson, J., 1984. Dictionary of Geological Terms: Third Edition.

Bemis, S., and Wallace, W., 2007. Neotectonic framework of the north-central Alaska Range foothills. , in Ridgway, K.D., Trop, J.M., Glen, J.M.G., and O'Neill, J.M., editors, Tectonic growth of a collisional continental margin: Crustal evolution of southern Alaska: Geological Society of America Special Paper 431, 551-574.

Bemis, S., Carver, G., and Koehler, R., 2012. The Quaternary thrust system of the northern Alaska Range. Geosphere 8, 196-205.

Benowitz, J., Layer, P., Armstrong, P., Perry, S., 3, Haeussler, P., Fitzgerald, P., and VanLaningham, S., 2011. Spatial variations in focused exhumation along a continental-scale strike-slip fault: The Denali fault of the eastern Alaska Range. *Geosphere* 7, 455–467.

Benowitz, J., Layer, P.W., VanLaningham, S., 2013. Persistent Long-Term (~24 Ma) Exhumation in the Eastern Alaska Range Constrained by Stacked Thermochronology. Geological Society of London Special Volume.

Berger, A., Gulick, S., Spotila, J., Upton, P., Jaeger, J., Chapman, J., Worthington, L., Pavliss, T., Ridgway, K., Willems, B., and Mcaleer, R., 2008. Quaternary tectonic response to intensified glacial erosion in an orogenic wedge. Nature Geoscience 1, 793-799.

Brocklehurst, S., and Whipple, K., 2006. Assessing the relative efficiency of fluvial and glacial erosion through simulation of fluvial landscapes. Geomorphology 75, 283–299.

Brook, M., Kirkbride, M., and Brock, B., 2006. Quantified time scale for glacial valley cross-profile evolution in alpine mountains. Geology 34, 637–640.

Brozovic, N., Burbank, D.W., Meigs, A.J., 1997. Climatic limits on landscape development in the northwestern Himalaya. Science 276, 571-574.

Burbank, D., and Anderson, R., 2011. Tectonic Geomorphology, 2nd. Ed.

Chen, Y., Sung, Q., and Cheng, K., 2003. Along-strike variations of morphotectonic features in the Western Foothills of Taiwan: tectonic implications based on stream-gradient and hypsometric analysis. Geomorphology 56, 109–137.

Csejtey, B., Mullen, M.W., Cox, D.P., and Stricker, G.D., 1992, Geology and geochronology of the Healy Quadrangle, south-central Alaska: U.S. Geological Survey Miscellaneous Investigations 1191, 63 p., 1 sheet, scale 1:250,000.

Daly, C., Neilson, R., and Phillips, D., 1994. A Statistical-Topographic Model for Mapping Climatological Precipitation over Mountainous Terrain. Journal of Applied Meteorology 33, 140-158.

Delcaillau, B., Carozza, J., and Laville, E., 2006. Recent fold growth and drainage development: The Janauri and Chandigarh anticlines in the Siwalik foothills, northwest India. Geomorphology 76, 241–256.

Denny, 2013, Identifying areas of neotectonic activity using radar remote sensing in the northern foothills of the Alaska Range. University of Alaska Fairbanks M.S. thesis.

ESRI, GIS Dictionary. <http://support.esri.com/en/knowledgebase/GISDictionary>

Fitzgerald, P., Sorkhabi, R., Redfield, T., and Stump, E., 1995. Uplift and denudation of the central Alaska Range: A case study in the use of apatite fission track thermochronology to determine absolute uplift parameters. Journal of Geophysical Research 100, 20175–20191.

Haeussler, P., 2008, An overview of the neotectonics of interior Alaska: Far-field deformation from the Yakutat microplate collision, in Freymueller, J., Haeusseler, P.,Wesson, R., and Ekstrom, G., eds., Active tectonics and seismic potential of Alaska: American Geophysical Union monograph 179, p. 83-108.

Harbor, J., 1992, Numerical modeling of the development of U-shaped valleys by glacial erosion: Geological Society of America Bulletin, v. 104, 1364–1375.

Hickman, R., Sherwood, K., and Craddock, C., 1990. Structural evolution of the early Tertiary Cantwell basin, south-central Alaska. Tectonics 9, 1433–1449.

Kienholz, C., 2013. Personal communication.

Koons, P., 1994. Three-dimensional critical wedges: tectonics and topography in o blique collisional orogens. Journal of Geophysical Research 99 (B6), 12301-12315.

Lesh, M., and Ridgway, K., 2007. Geomorphic evidence of active transpressional deformation in the Tanana foreland basin, south-central Alaska, in Ridgway, K.D., Trop, J.M., Glen, J.M.G., and O'Neill, J.M., editors, Tectonic growth of a collisional continental margin: Crustal evolution of southern Alaska: The Geological Society of America Special Paper 431: 573-593.

MacGregor, K., Anderson, R., and Anderson, S., 2000. Numerical simulations of glacial-valley longitudinal profile evolution: Geology 28, 1031– 1034.

Manley, W., and Kaufman, D., 2002. Alaska PaleoGlacier Atlas: Institute of Arctic and Alpine Research (INSTAAR), University of Colorado, http://instaar.colorado.edu/QGISL/ak_paleoglacier_atlas, v. 1.

Meigs, A., and Sauber, J., 2000. Southern Alaska as an example of the long-term consequences of mountain building under the influence of glaciers. Quaternary Science Reviews 19, 1543-1562.

Mitchell, S., and Montgomery, D., 2006. Influence of a glacial buzzsaw on the height and morphology of the Washington Cascade Range, Washington State, USA. Quaternary Research 65, 96-107.

Molnar, P., and England, P., 1990. Late Cenozoic uplift of mountain ranges and global climatic changes: chicken or egg? Nature 346, 29-34.

Montgomery, D., Balco, G., and Willett, S., 2001. Climate, tectonics, and the morphology of the Andes. Geology 29, 579-582.

Nokleberg, W.J., Aleinikoff, J.N., Lange, I.M., Silva, S.R., Miyaoka, R.T., Schwab, C.E., and Zehner, R.E., 1992. Preliminary geologic map of the Mount Hayes quadrangle, eastern Alaska Range, Alaska: U.S. Geological Survey Open-File Report 92-594, 39 p., 1 sheet, scale 1:250,000.

Oskin, M., and Burbank, D., 2005. Alpine landscape evolution dominated by cirque retreat. Geology 33, 933-936.

Péwé, T., 1975. Quaternary geology of Alaska. USGS Professional Paper 835.

Plafker, G., Moore, J., and Winkler, G., 1994. Geology of the southern Alaska margin, in Plafker, G., and Berg, H.C., eds., The Geology of Alaska, Geological Society of America, Boulder, Colorado, The Geology of North America, v. G-1, 389-450.

Ramsey, L., Walker, R., and Jackson, J., 2008. Fold evolution and drainage development in the Zagros mountains of Fars province, SE Iran. Basin Research 20, 23–48.

Ridgway, K., Trop, J., Nokleberg, W., Davidson, C., and Eastham, K., 2002. Mesozoic and Cenozoic tectonics of the eastern and central Alaska Range: Progressive basin development and deformation in a suture zone: Geological Society of America Bulletin 114, 1480–1504.

Schumm, S., 1986. Alluvial river response to active tectonics. In: Studies in National Research Council (Ed.), Active Tectonics. National Academy Press, Studies in Geophysics, Washington, D.C, 80–94.

Spotila, J., 2012. Influence of drainage divide structure on the distribution of mountain peaks. GEOLOGY 40, 855–858.

Spotila, J., and Berger, A., 2010. Exhumation at orogenic indentor corners under long-term glacial conditions: Example of the St. Elias orogen, Southern Alaska. Tectonophysics 490, 241–256.

Tomkin, J., and Roe, G., 2007.Climate and tectonic controls on glaciated critical-taper orogens. Earth Planetary Science Letters 262, 385–397.

Trop, J., and Ridgway, K., 2007. Mesozoic and Cenozoic tectonic growth of southern Alaska: A sedimentary basin perspective, in Ridgway, K.D., Trop, J.M., Glen, J.M.G., and O'Neill, J.M., eds., Tectonic growth of a collisional continental margin: Crustal evolution of Southern Alaska: Geological Society of America Special Paper 431, 5-94.

Ward, D., Anderson, R., and Haeussler, P., 2012. Scaling the Teflon Peaks: Rock type and the generation of extreme relief in the glaciated western Alaska Range. Journal of Geophysical Research 117, 1-20.

Whipple, K., 2009. The influence of climate on the tectonic evolution of mountain belts. Nature Geoscience 2, 97-104.

Wilson, F.H., Dover, J.H., Bradley, D.C., Weber, F.R., Bundtzen, T.K., and Haeussler, P.J., 1998. Geologic map of Central (Interior) Alaska. USGS Open-file report 98-133.